NMDA receptors potentiate activity-dependent dendritic release of neuropeptides from hypothalamic neurons

Soledad Pitra[1], Meng Zhang[1], Edmund Cauley[2] and Javier E. Stern[1] (iD)

[1] Medical College of Georgia, Augusta University, Augusta, GA, USA
[2] Department of Pharmacology and Physiology, George Washington University, Washington, DC, USA

Edited by: Ian Forsythe & Jean-Claude Béïque

Key points

- Using 'sniffer' cell biosensors, we evaluated the effects of specific firing patterns and frequencies on activity-dependent somatodendritic release of vasopressin from paraventricular nucleus neurones.
- Somatodendritic release of vasopressin was rarely observed during continuous firing but was strengthened by clustered activity. Moreover, release evoked at any given frequency was robustly potentiated by NMDA receptor (NMDAR)-mediated firing.
- Differently from axonal release, NMDAR activation was necessary for somatodendritic release to occur at physiological firing frequencies, acting thus as a gating mechanism by which activity-dependent release from these two neuronal compartments could be independently regulated.
- The NMDAR-mediated potentiation was independent of a specific firing pattern and was not accompanied by increased spike broadening, but correlated with higher dendritic Ca^{2+} levels.
- Our studies provide fundamental novel information regarding stimulus–secretion coupling at somatodendritic compartments, and shed light into mechanisms by which activity-dependent release of neuronal signals from axonal terminals and dendrites could be regulated in a spatially compartmentalized manner.

Abstract   Dendrites are now recognized to be active transmitting neuronal compartments subserving complex brain functions, including motor behaviours and homeostatic neurohumoral responses. Still, the precise mechanisms underlying activity-dependent release of dendritic signals, and how dendritic release is regulated independently from axonal release, remains largely unknown. We used 'sniffer' biosensor cells to enable the measurement and study of activity-dependent dendritic release of vasopressin (VP) from hypothalamic neurones in brain slices. Sniffer$_{VP}$ responses were dose-dependent, with a threshold detection level of 0.5 nM for VP, being thus a highly sensitive tool to detect endogenous physiological levels of the neuropeptide. Somatodendritic release of VP was rarely observed in response to a burst of action potentials fired in continuous mode, but was strengthened by clustered firing activity. Moreover, release evoked at any given frequency was robustly potentiated when firing was triggered by NMDA
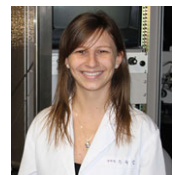
receptor (NMDAR) activation. Differently from axonal release, NMDAR activation was necessary for dendritic release to occur at physiological firing frequencies. Thus, we propose that NMDARs may act as a gating mechanism by which activity-dependent release from these two neuronal compartments can be independently regulated. The NMDAR-mediated potentiation of dendritic release was independent of a particular action potential waveform, firing pattern evoked, or a more pronounced spiked broadening, but correlated with higher dendritic Ca^{2+} levels. Overall, our studies provide fundamental novel information regarding stimulus–secretion coupling at neuronal dendrites, and shed light into mechanisms by which activity-dependent release of neuronal signals from axonal terminals and dendrites can be regulated in a spatially compartmentalized manner.

Corresponding author J. E. Stern: Neuroscience Institute, Georgia State University, 125 Decatur St. SE, Atlanta, GA 30303, USA.   Email: jstern@gsu.edu

Introduction

Transfer of information in the brain was classically considered a unidirectional process, in which dendrites acted as passive receptive fields, integrating and transferring signals to the soma and then to the axon, leading ultimately to release of a chemical transmitter. It is now well accepted, however, that dendrites possess active properties, that they can transmit action potentials in the reverse direction (Stuart *et al.* 1997), and that they can also actively release signals (Cheramy *et al.* 1981; Toida *et al.* 1994; Ludwig & Leng, 2006; Kennedy & Ehlers, 2011; Rice & Patel, 2015), particularly neuropeptides from dendritic large dense-core vesicles (LDCVs). Thus, dendrites act not only as receivers, but also as transmitting cell compartments in information processing in the brain.

Somatodendritic release of neuropeptides is now recognized to play critical physiological roles, including autoregulation of neuronal activity (Ludwig & Leng, 1997, 2006), generation of multimodal homeostatic responses (Son *et al.* 2013), and complex behavioural responses as well (Engelmann *et al.* 1994; Ludwig & Leng, 2006; Albers, 2015). Nonetheless, most available knowledge on stimulus–secretion coupling originated almost exclusively from studies on synaptic vesicles and classical neurotransmitters at axonal terminals. Thus, fundamental information regarding the precise mechanisms governing stimulus–secretion coupling of dendritic LDCVs in the CNS remains largely unexplored.

Magnocellular neurosecretory cells (MNCs) of the hypothalamic supraoptic nucleus (SON) and paraventricular nucleus (PVN) are one of the best-characterized prototypes of dendritic neurotransmitter release (Morris & Ludwig, 2004; Ludwig & Leng, 2006). In addition to releasing their vasopressin (VP) and oxytocin (OT) cargo from neurohypophysial axon terminals, MNCs also store and release neuropeptides from their somata and dendrites. Somatodendritic neuropeptide release from MNCs is activity-dependent, involves Ca^{2+}-dependent exocytosis of LDCVs, and importantly, can be regulated autonomously from axonal release (Ludwig *et al.* 2005; Ludwig & Leng, 2006). Somatodendritic release of VP and OT acts as a powerful feedback signal by which MNCs autoregulate their own activity (Ludwig & Leng, 1997; Gouzenes *et al.* 1998). Moreover, we recently showed that somatodendritically released VP acts as a diffusible interpopulation signal to coordinate the activity of neurosecretory and sympathetic neurones, and to mediate the generation of multimodal homeostatic responses by the PVN (Son *et al.* 2013). Despite the physiological relevance of dendritically released OT and VP, information about the precise mechanisms that regulate their release is missing, due in part to the lack of efficient tools available to measure neuropeptide release with high spatiotemporal resolution and sensitivity.

In the present study, we used MNCs as a model system to study stimulus–secretion coupling mediating dendritic release of LDCVs. To monitor somatodendritic release of VP *in situ* and in real time, we used 'sniffer' biosensor cells consisting of genetically engineered Chinese hamster ovary (CHO) cells that expressed VP or OT receptors along with a fluorescent Ca^{2+} indicator. Using sniffer biosensors in conjunction with patch-clamp electrophysiology and confocal Ca^{2+} imaging in PVN slices from enhanced green fluorescent protein (eGFP)–VP transgenic rats, we assessed the impact of varying firing frequencies and firing patterns on dendritic release of VP. Moreover, given that glutamate, acting mostly on NMDA receptors (NMDARs), is a critical neurotransmitter driving firing activity in MNCs (Hu & Bourque, 1992; Fleming *et al.* 2011), and based also on the fact that NMDAR activation was previously shown to efficiently evoke dendritic release of VP and OT (de Kock *et al.* 2004; Son *et al.* 2013), we assessed the role of NMDAR-evoked firing in regulating the efficacy of dendritic release of VP from MNCs. We found that neuropeptide dendritic release efficacy is dependent on the pattern (but not the total number or

frequency) of somatic firing activity. We also uncovered that for any given frequency, firing activity evoked by NMDA receptor (NMDAR) activation robustly boosted dendritic release of VP and shortened its release latency, an effect that correlated with larger dendritic Ca^{2+} signalling compared to other firing modalities. Differently from what was previously shown for axonal release, our studies demonstrate that activation of NMDARs was necessary for dendritic release to occur at physiological firing frequencies typically displayed by VP neurones. Thus, we propose that NMDARs in MNCs may act as a 'gating' mechanism, contributing to the autonomous activity-dependent regulation of neuropeptide release from dendritic and axonal compartments.

Methods

Animals

All procedures were performed in agreement with guidelines of the Augusta University and Georgia State University Institutional Animal Care and Use Committee and were approved by the respective committees (approval reference no. 2008-0133). Male heterozygous transgenic eGFP–VP Wistar rats (3–5 weeks old, $n = 32$) were used (Ueta *et al.* 2005). Rats were housed in rooms with constant temperature of 22–24°C and under a controlled light–dark cycle (12 h–12 h), with normal rat chow and drinking water *ad libitum*.

Slice preparation

Hypothalamic brain slices were prepared according to methods previously described (Son *et al.* 2013). Briefly, rats were anaesthetized with pentobarbital (50 mg kg^{-1} I.P.); brains were dissected out and hypothalamic coronal slices (240 μm) containing the PVN were cut in an oxygenated ice-cold artificial cerebrospinal fluid (aCSF), containing (in mM): 119 NaCl, 2.5 KCl, 1 MgSO$_4$, 26 NaHCO$_3$, 1.25 NaH$_2$PO$_4$, 20 D-glucose, 0.4 ascorbic acid, 2 CaCl$_2$ and 2 pyruvic acid; pH 7.3; 295 mOsm). Slices were placed in a holding chamber containing aCSF and kept at room temperature until used.

Electrophysiology

Hypothalamic slices were transferred to a recording chamber and superfused with continuously bubbled (95% O$_2$–5% CO$_2$) aCSF (30–32°C) at a flow rate of $\sim$3.0 ml min^{-1}. Thin-walled (1.5 mm OD, 1.17 mm ID) borosilicate glass (G150TF-3; Warner Instruments, Sarasota, FL, USA) was used to pull patch pipettes (3–5 MΩ) on a horizontal micropipette puller (P-97; Sutter Instruments, Novato, CA, USA). The internal solution contained the following (in mM): 135 potassium gluconate, 0.2 EGTA, 10 Hepes, 10 KCl, 0.9 MgCl$_2$,

4 Mg^{2+}-ATP, 0.3 Na$^+$-GTP and 20 phosphocreatine (Na$^+$); pH was adjusted to 7.2–7.3 with KOH. Unless otherwise indicated, all recordings were obtained from identified VP neurones in the lateral magnocellular subdivision of the PVN, using an Axopatch 200B amplifier (Axon Instruments, Foster City, CA, USA), and with a combination of fluorescence and infrared differential interference contrast (DIC) illumination. Recorded neurones were verified as MNCs based on the presence of a robust transient outward rectification upon depolarization from hyperpolarized membrane potentials (Luther & Tasker, 2000). The voltage output was digitized at 16-bit resolution and at 10 kHz and was filtered at 2 kHz (Digidata 1440A; Axon Instruments). Data were discarded if the series resistance was not stable throughout the entire recording ($>$20% change). Firing activity was evoked either via current injection through the patch pipette (10–100 pA) or by focally delivering NMDA via a patch pipette positioned within 10–20 μm from the recorded cell (picospritzer, 3–5 PSI, 10 μM NMDA).

For direct current injection, firing activity was evoked either in a continuous mode (continuous firing; CF) (depolarizing pulses of increasing duration, between 0.05 and 3 s) or in a repetitive bursting mode (repetitive bursting firing; RBF), consisting of five consecutive stimuli, 0.5 s duration each, 0.2 s interval. We selected this particular protocol based on our previous work showing that five consecutive bursts were necessary to evoke an interpopulation crosstalk between VP MNCs and presympathetic PVN neurons, mediated by somatodendritically released VP (Son *et al.* 2013). For NMDA applications, the duration of the puff was varied (100–1000 ms) in order to achieve a similar number of action potentials evoked via direct current injection). Following this procedure, we found that moving the puff pipette 20–25 μm (i.e. about 1–2 MNC body diameters) away from its original position failed to evoke a Ca^{2+} response in the patched neurone. Moreover, in a few control cases ($n = 4$) in which slices were preloaded with the membrane-permeant Ca^{2+} sensitive dye Fluo-5 AM (10 μM), using similar approaches as previously reported (Filosa *et al.* 2012), and in which a cluster of viable and loaded MNCs were close to each other, we found that Ca^{2+} responses were elicited only in the MNCs to which the puff pipette was targeted. These control experiments, along with our results showing that somatodendritic release of VP in response to NMDA puff was almost completely blocked when the patched VP neurones were dialysed with BAPTA (see more in Results), support that a single MNC was sufficiently stimulated with NMDA to evoke a detectable Ca^{2+} response.

In some cases, the experimentally recorded burst of action potentials evoked was then applied as a voltage-clamp command to the same recorded neurone. The number and frequency of spikes evoked (spikes/s)

for the entire duration of each stimulating protocol was calculated. Spike broadening during a train of action potentials was calculated by measuring individual spike width (at 50% of peak), and was then normalized to the spike width of the first action potential in the train. Plots of relative spike width as a function of the spike number in the train were generated and then fit with a linear regression to calculate the rate of spike broadening. All electrophysiology analysis was performed using Clampfit (Axon Instruments) or MiniAnalysis (Synaptosoft, Fort Lee, NJ, USA) software. The number of evoked action potentials and their frequency (number of spikes/time) are reported. For RBF, reported values represent the total number of spikes in the five elicited bursts, and the frequency represents the mean frequency calculated for each burst. As indicated throughout the text, drugs were either bath-applied, focally applied with a picospritzer, or delivered as a bolus (0.5 ml) into the perfusion line.

Sniffer$_{VP}$ and sniffer$_{OT}$ cells

CHO cells were transfected with pcDNA3.1+ containing human V1a or OT receptors cloned in at *Eco*RI (5′) and *Xho*I (3′) (plasmid obtained from Missouri S&T cDNA Resource Center, Rolla, MO, USA) using lipofectamine, and stable overexpression was achieved by geneticin (500 mg ml^{-1}) selection (Pinol *et al.* 2014). V1aR/OTR-expressing CHO cells (sniffer$_{VP}$ and sniffer$_{OT}$ cells, respectively) were then plated and transiently transfected to express the red fluorescent genetically encoded Ca^{2+} indicator (R-GECO; GenScript, Piscataway, NJ, USA) with Fugene HD reagent (Promega, Madison, WI, USA). To examine the selectivity, affinity and responsiveness of these V1aR/OTR-expressing CHO cells, we measured their Ca^{2+} dose–response relationship following exogenously delivered VP and OT (10–100 nM). To study sniffer cell responsiveness to activity-dependent, endogenously released VP and OT, sniffer cells were treated with trypsin (0.05 %), resuspended in aCSF and then plated directly onto a brain slice containing PVN eGFP–VP neurones. PVN neurones were stimulated as described above, and fluorescent Ca^{2+} responses were monitored in surrounding sniffer cells contained within the lateral magnocellular subdivision of the PVN. In a series of pilot studies, we determined that ∼50–70% of the plated sniffer cells that were detectable based on their basal fluorescence level were responsive to their respective agonists (e.g. OT or VP, see Fig. 1*A*). It is also important to know that Ca^{2+} responses were also evoked following different stimulation protocols in sniffer cells that had no detectable basal fluorescence (e.g. Fig. 2*C*, cell no. 1). Finally, the density of plated sniffer cells varied across the slice. To circumvent these limitations and be consistent across studies, we restricted our experiments to patched eGFP–VP neuro-

nes that had at least five fluorescently visible sniffer cells in their vicinity (∼10 on average). The overall mean distance from the centre of the patched eGFP–VP somata to the responsive sniffer$_{VP}$ cells was 46.6 ± 6.7 μm (range 5–122 μm).

Confocal Ca^{2+} imaging and analysis of sniffer cells and patched MNCs

Sniffer$_{VP}$ and sniffer$_{OT}$ cells, as well as Fluo-5F pentapotassium salt (50 μM; Thermo Fisher Scientific, Waltham, MA, USA)-loaded MNCs (Stern & Potapenko, 2013), were imaged using the Andor Technology Revolution system (iXON EMCCD camera with the Yokogawa CSU 10 (Tokyo, Japan), confocal scanning unit; Belfast, UK), at a rate of 4 Hz, using an excitation light of 488 nm and emitted light at >495 nm (Fluo-5F). Basal fluorescence in sniffer cells was variable, likely due to multiple factors including variability in plasmid transfection efficacy and actual basal cytoplasmic Ca^{2+} levels, among others. Thus, for quantitative measurements, we used fractional fluorescence (F/F_0), a standardized and widely used approach to quantitatively assess relative changes in fluorescence. F/F_0 within each sniffer cell was determined by dividing the fluorescence intensity (F) within a region of interest by a baseline fluorescence value (F_0) determined from 50 images before stimulation (Stern & Potapenko, 2013). Importantly, despite this intrinsic variability, we found in a subset of experiments no correlation between basal sniffer cell fluorescence and the magnitude of the cell's Ca^{2+} response to the various firing modalities used in this study ($r^2 = 0.02$, $n = 31$). We also noticed that some sniffer cells showed intrinsic oscillatory Ca^{2+} activity. Thus, before each experiment, baseline image traces were obtained (5–10 min) to identify oscillatory cells, which were discarded from analysis. Imaging data were analysed using ImageJ software (NIH).

Neuronal dendritic Ca^{2+} responses (F/F_0) to the various stimulation protocols evoked in each neurone were quantified and normalized by the number of action potentials evoked. To better display changes in fluorescence levels, images were converted to pseudo-colour using ImageJ.

Drugs

All drugs, with the exception of tetrodotoxin (TTX, Alomone Labs, Jerusalem, Israel), were purchased from Sigma-Aldrich (St Louis, MO, USA).

Statistical analysis

All values are expressed as means ± SEM. Student's paired *t* test was used to compare the effects of drug

treatment. One- or two-way ANOVA with the Bonferroni or Dunnet's *post hoc* test was used as stated. Differences were considered significant at $P < 0.05$ and n refers to the number of sniffer cells. EC_{50} values were obtained by fitting dose–response data with a non-linear function. All statistical analyses were conducted using Prism (GraphPad Software, San Diego, CA, USA).

Results

Quantitative detection of VP and OT with sniffer biosensor cells

CHO cells that express V1a VP receptors (V1aRs) or OT receptors, along with the red fluorescent Ca^{2+} indicator R-GECO were used as VP- or OT-sensitive sniffer cells ($sniffer_{VP}$ and $sniffer_{OT}$), respectively. Binding of VP to V1aRs is known to evoke an inositol 1,4,5-trisphosphate-dependent release of Ca^{2+} from intracellular stores (Sabatier *et al.* 2004), which is

then visualized as an increase in R-GECO fluorescence within the $sniffer_{VP}$ cell. To determine the efficiency and sensitivity of this system, $sniffer_{VP}$ cells were first exposed to varying concentrations of VP. As shown in Fig. 1*A*, VP evoked robust increases in $sniffer_{VP}$ Ca^{2+} levels that were reproducible, with no significant changes in the magnitude of the response over time ($P = 0.8$, one-way ANOVA, $n = 4$, Fig. 1*Ba*). VP effects were dose-dependent, with an EC_{50} of 7.2 nM and an apparent threshold response of 0.5 nM (Fig. 1*Bb*). The magnitude of the $sniffer_{VP}$ Ca^{2+} response was also dependent on the proximity of the VP source to the CHO_{VP} cell ($P < 0.03$, one-way ANOVA, Fig. 1*Bc*).

Both VP and OT neuropeptides can bind V1aRs, though the sensitivity of the latter to OT is much lower compared to VP (Manning *et al.* 2012). We found that at concentrations of 5 and 50 nM, OT failed to evoke Ca^{2+} responses in $sniffer_{VP}$ cells. Even at 500 nM, OT responses were only $4.9 \pm 1.8\%$ of the response evoked by 50 nM VP on the same $sniffer_{VP}$ cells (500 nM OT:
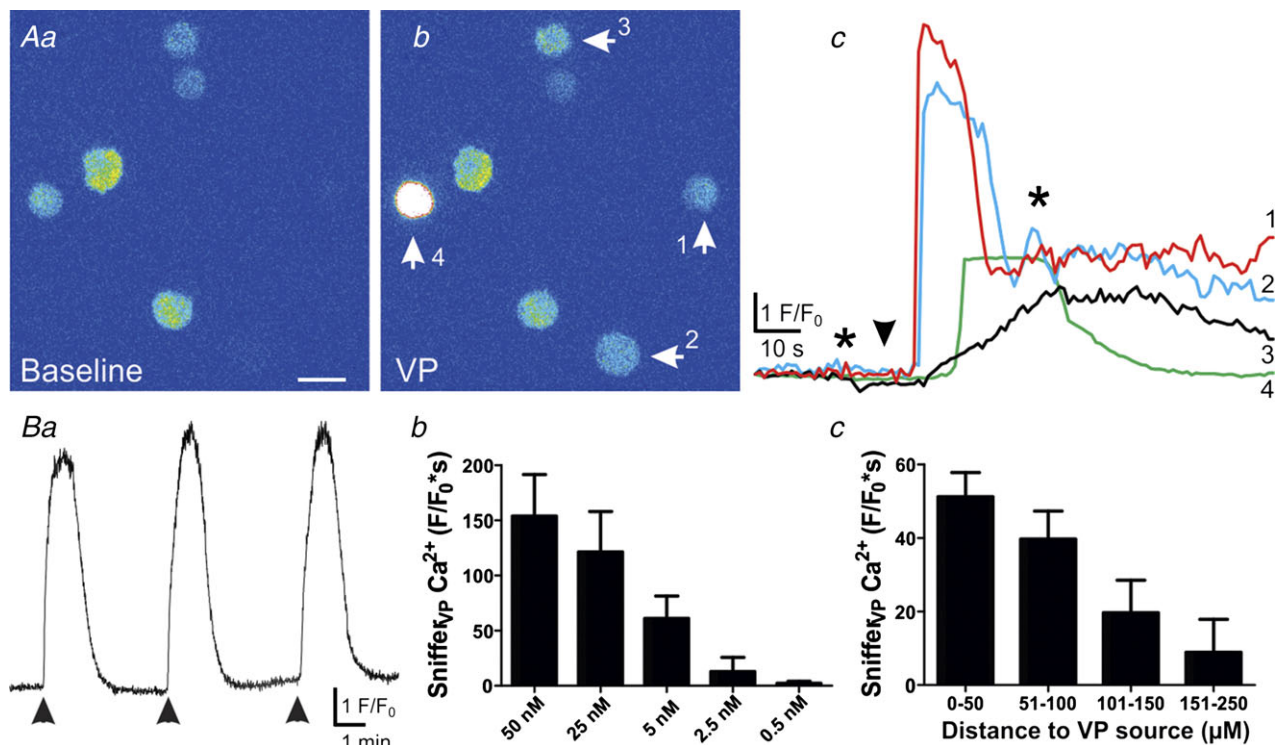

Figure 1. Validation of sniffer_VP cells as VP biosensors
A, pseudocolour images showing that $sniffer_{VP}$ basal intracellular Ca^{2+} concentration (*a*) was increased in 4 $sniffer_{VP}$ cells (arrows) following exogenous VP application (50 nM, bolus, *b*). A plot of these $sniffer_{VP}$ Ca^{2+} responses (F/F_0) over time is shown in *c*. The arrowhead indicates the time of VP application, and the asterisks correspond to the time points of the images shown in *a* and *b*. Note that in some cases (i.e. $sniffer_{VP}$ no. 1), basal fluorescence was almost indistinguishable from the background. Note also that since results are expressed as F/F_0, the brightest response (i.e. $sniffer_{VP}$ no. 4) does not correspond with the largest F/F_0 peak, since its basal fluorescence was also relatively high. *Ba*, the $sniffer_{VP}$ Ca^{2+} response was reproducible showing little decrement in response to repeated VP applications (2 min intervals). *Bb* and *c*, summary data showing that $sniffer_{VP}$ responses to VP were dose- (*b*, $n = 8$) and distance- (*c*, $n = 5$, bin = 50 μm) dependent. Changes in distance were accomplished by moving the puff pipette containing VP closer or farther away from the $sniffer_{VP}$ cells. Scale bar: 15 μm. [Colour figure can be viewed at wileyonlinelibrary.com]

$9.5 \pm 2.5 F/F_0$ s, $n = 10$ *vs.* 50 nM VP: 163.0 ± 7.5 F/F_0 s, $n = 29$, $P < 0.0001$). Conversely, a much more robust response to OT (5 nM) was observed in sniffer$_{OT}$ cells (180.3 ± 27.2 F/F_0 s, $n = 25$). Thus, sniffer$_{VP}$ cells display a high sensitivity and selectivity for VP. These results are in large agreement with a recent work published at the time

of submission of this manuscript, in which similar sniffer cells were generated using human embryonic kidney (HEK) cells transfected with GCaMP6m as the Ca^{2+} sensor (Zaelzer *et al.* 2018), and further confirm the use of the sniffer cell approach as an efficient and sensitive tool to quantitatively detect oxytocin and vasopressin release.
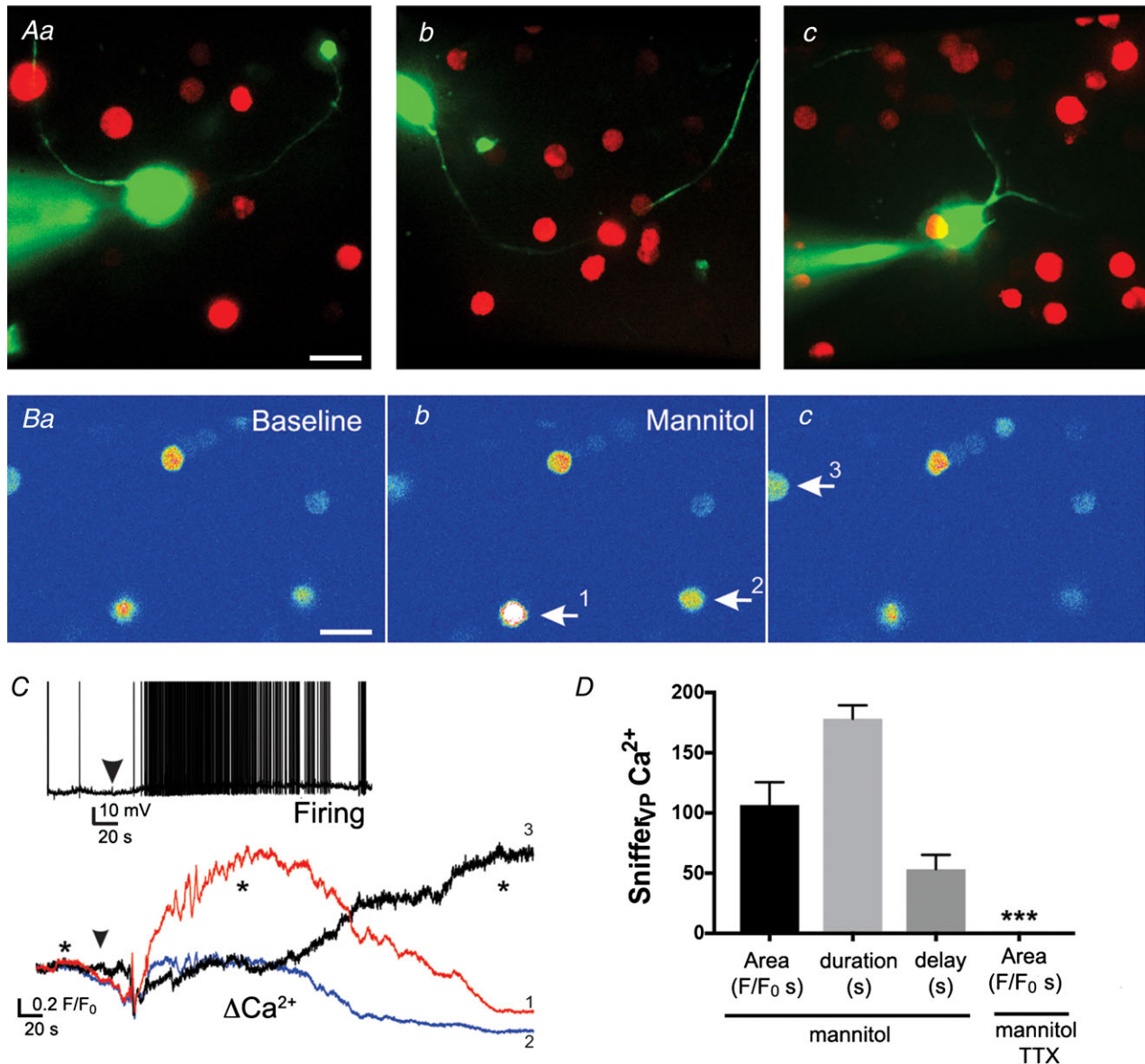
Figure 2. Sniffer$_{VP}$ cells detect endogenous somatodendritic release of VP evoked by an osmotic challenge

Aa–c, samples of patched eGFP–VP neurones loaded with Alexa 488 surrounded by sniffer$_{VP}$ cells. *B*, pseudocolour images showing baseline (*a*) and increased Ca^{2+} levels in 3 different sniffer$_{VP}$ cells (arrows, *b* and *c*) after application of mannitol (bolus, +10 mOsm). *C*, plot of changes in Ca^{2+} levels over time in the 3 sniffer$_{VP}$ cells shown in *B* in response to the osmotic stimulation (arrowhead). Asterisks correspond to the time points of the images shown in *Ba* and *c*. Inset, sample of the increased firing discharge in a patched eGFP–VP neurone in response to the osmotic stimulation (arrowhead). *D*, summary data of the mean area, duration and delay of the sniffer$_{VP}$ cell responses to mannitol in control ACSF ($n = 16$ obtained from 4 slices) and in the presence of TTX ($n = 31$ cells from 7 slices). ***$P < 0.0001$ vs. mannitol. Scale bars: 15 μm. [Colour figure can be viewed at wileyonlinelibrary.com]

Detection of activity-dependent somatodendritic release of neuropeptides from the population of VP PVN neurones using sniffer biosensor cells

To determine if in our conditions sniffer$_{VP}$ cells could detect a mean endogenous 'population' somatodendritic release of VP, sniffer$_{VP}$ cells were enzymatically dispersed and plated onto PVN slices containing genetically identified VP neurones (i.e. eGFP–VP, Fig. 2*A*, see more details in Methods) that were challenged with an osmotic stimulation (bolus, mannitol, +10 mOsm), a condition known to evoke activity-dependent somatodendritic release of VP (Ludwig *et al.* 1994, 1995). We simultaneously monitored the electrical activity of a patched eGFP–VP neurone in the PVN, which acted as a proxy to the VP population, as well as the Ca^{2+} responses in surrounding sniffer$_{VP}$ cells. Exposing PVN slices to the acute osmotic challenge evoked firing activity in the patched VP neurones (total mean number of evoked spikes during the stimulation: 215.0 ± 121.1; mean firing frequency: 3.6 ± 0.9 Hz; delay from stimulation to onset of firing: 30.0 ± 10.4 s; $n = 4$ VP neurones) that subsequently evoked Ca^{2+} responses in surrounding sniffer$_{VP}$ cells (Fig. 2*B* and *C*) (106.5 ± 19.1 F/F_0 s; $n = 16$ sniffer cells; mean delay from stimulation: 76.8 ± 14.4 s). Importantly, sniffer$_{VP}$ Ca^{2+} responses were almost completely blocked in slices preincubated with 1 μM TTX (0.31 ± 0.17 F/F_0 s; $n = 31$ cells from 7 slices, $P < 0.0001$ *vs.* control, Fig. 2*D*). Sniffer$_{VP}$ responses to the osmotic challenge displayed relatively slow kinetics and were long lasting (mean Ca^{2+} duration: 178.2 ± 11.3 s), likely as a result of the osmotically driven asynchronous release of VP (Brown & Bourque, 2006) from multiple different sources.

Clustered but not continuous firing pattern evokes somatodendritic release of VP from individual neurones

We then aimed to determine whether and how different patterns of firing activity influenced stimulus–secretion coupling of somatodendritic LDCV's from individual VP neurones. To this end, we patched eGFP–VP neurones in PVN slices containing sniffer$_{VP}$ cells. Patched neurones were dialysed with Alexa 488 (50 μM) in order to better visualize their dendrites (see examples in Fig. 2*A*). As shown in the representative example in Fig. 3*A*, depolarizing pulses of increasing durations (0.05–3 s) evoked action potential activity in a continuous firing (CF) pattern. The range of the number of action potentials evoked in this modality was 2–120, with frequencies ranging from 14.7 to 40 Hz. Yet, no Ca^{2+} responses in neighbouring sniffer$_{VP}$ cells were observed in response to these depolarizing pulses. A similar lack of sniffer$_{VP}$ responses to CF pattern activity was observed in four

independent experiments in which similar depolarizing protocols were applied to patched VP neurones.

We recently reported that repetitive bursting firing (RBF) pattern in VP neurones engaged a functional cross-talk with neighbouring presympathetic neurones, which resulted from the diffusion of dendritically released VP in the extracellular space (Son *et al.* 2013). We found here that when the same VP neurone that failed to release VP in CF mode was subjected to the RBF pattern previously used (Son *et al.* 2013) (5 consecutive stimuli, 0.5 s duration, 0.2 s interval), a Ca^{2+} response in a neighbouring sniffer$_{VP}$ cell was observed (2.3 F/F_0 s, representative example in Fig. 3*B*). Another example showing sniffer$_{VP}$ Ca^{2+} responses following RBF pattern activity in a VP neurone (149 action potentials, 49.7 Hz) is shown in Fig. 3*C* and *D*. A mean summary of the magnitude, duration and delay of sniffer$_{VP}$ Ca^{2+} responses following RBF activity is shown in Fig. 3*E*. The mean number of responsive sniffer$_{VP}$ cells per eGFP–VP neurone stimulated with the RBF modality ($n = 11$) was 1.1 ± 0.13.

The number of evoked action potentials and their intraburst frequency during RBF varied greatly from cell to cell. However, we found no significant correlation between the magnitude of the sniffer$_{VP}$ cell response with either the total number of action potentials or the mean action potential frequency ($r^2 = 0.04$ for both parameters, $n = 31$ sniffer$_{VP}$ cells associated to 11 stimulated eGFP–VP neurones).

### NMDA receptor-evoked firing potentiates somatodendritic release of VP

The results above suggest that clustered firing is more efficient in evoking somatodendritic release of VP when compared to a continuous pattern of activity. Activation of NMDARs in MNCs also evokes clustered activity (Hu & Bourque, 1992; Bains & Ferguson, 1997; Gagnon *et al.* 2014) and we recently showed that NMDAR-evoked firing activity in VP neurones more efficiently engaged a neurosecretory-presympathetic interpopulation coupling in the PVN, compared to firing activity evoked by direct current injection (Son *et al.* 2013). Thus, to directly assess the efficacy and kinetics of somatodendritically released VP following NMDAR activation, patched eGFP–VP neurones ($n = 10$) in PVN slices containing sniffer$_{VP}$ cells were focally stimulated with NMDA (picospritzer, 10 μM). To minimize the possibility of multiple MNCs stimulation, we set our puff protocols according to control experiments we previously run to minimize this possibility (see Methods and more below).

As shown in the representative example of Fig. 4, NMDA evoked a burst of action potentials in the patched VP neurone (28 spikes, 43.8 Hz), as well as a clear Ca^{2+} response in three surrounding sniffer$_{VP}$ cells, which occurred with a delay of ~1 s after stimulation

(Fig. 4*B* and *D*). A summary of the mean magnitude, duration and delay of Ca^{2+} responses in sniffer$_{VP}$ cells following NMDAR-evoked firing is shown in Fig. 4*E*. The mean number of responsive sniffer$_{VP}$ cells per stimulated eGFP–VP neurone was 2.2 ± 0.45. Similar to the responses evoked with the RBF pattern, we found no significant correlation between the magnitude of the sniffer$_{VP}$ cell response with either the total number of action potentials
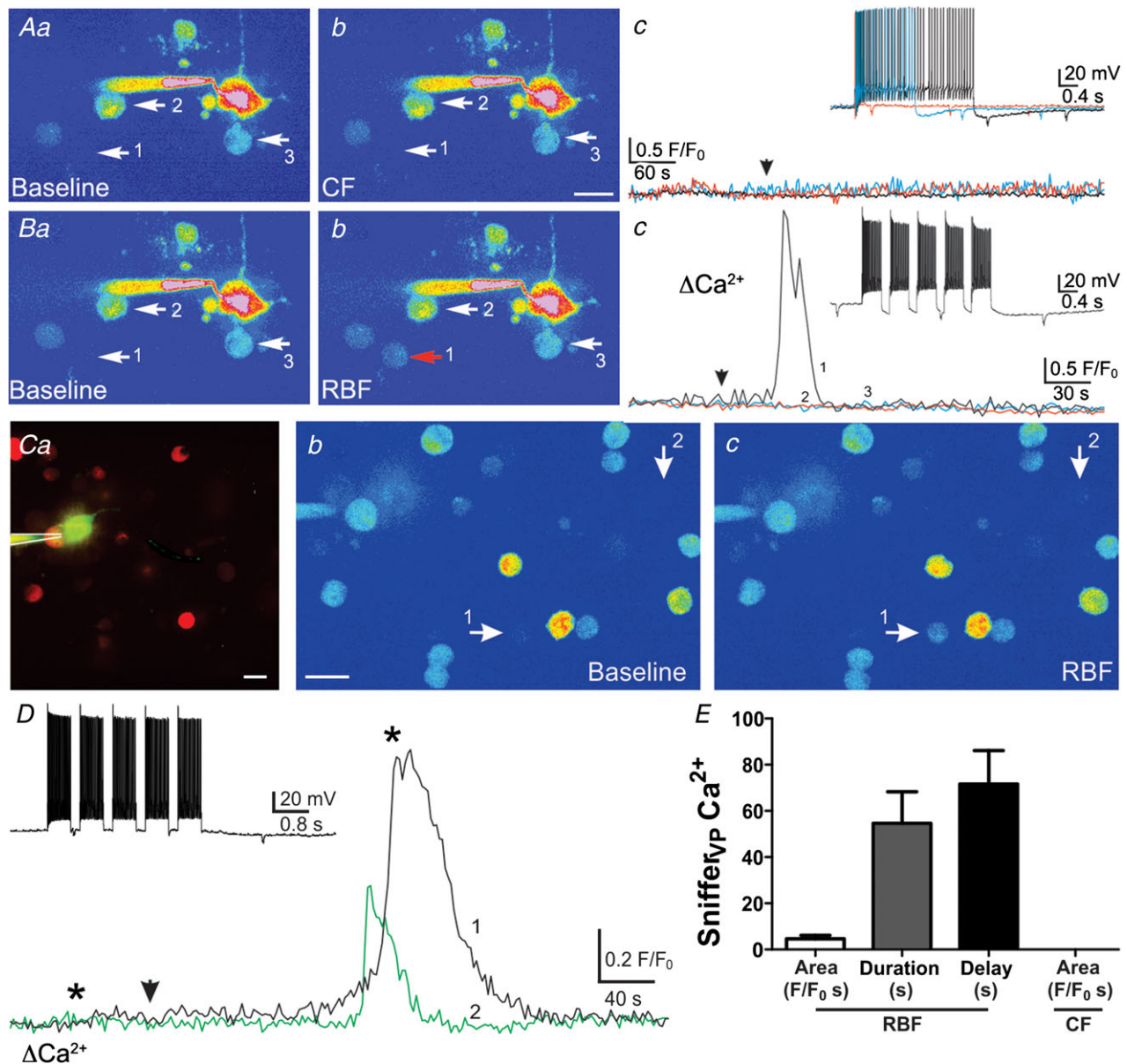
Figure 3. Clustered but not continuous firing pattern evokes somatodendritic release of VP from individual neurones

A, pseudocolour image showing a patched eGFP–VP neurone surrounded by sniffer$_{VP}$ cells (arrows, *a*, note the lack of sniffer$_{VP}$ cell responses (*b* and *c*) when continuous firing (CF) activity was evoked in the patched neurone (arrowhead) using depolarizing pulses of increasing duration (*c*, inset). *Ba* and *b*, when the same neurone from *A* was then stimulated to evoke a repetitive bursting firing pattern (RBF, inset, *Bc*), a robust Ca^{2+} increase was observed in one of the sniffer$_{VP}$ cells (*Bc*, *Bb*) approximately 30 s after stimulation (arrowhead). *Ca*, fluorescence image of a different patched eGFP–VP neurone loaded with Alexa 488 surrounded by sniffer$_{VP}$ cells. *Cb* and *c*, corresponding pseudocolour images showing baseline (*b*) and sniffer$_{VP}$ Ca^{2+} responses (*c*, arrows) when the patched neurone was stimulated to generate a RBF pattern (*D*, inset). *D*, plot of the sniffer$_{VP}$ Ca^{2+} response over time to the RBF stimulation (arrowhead). Asterisks correspond to the time points of the images shown in *Cb* and *c*. *E*, summary data of the mean area, duration and delay of sniffer$_{VP}$ responses to RBF stimulation ($n = 31$ sniffer$_{VP}$ cells). Scale bars: 15 μm. [Colour figure can be viewed at wileyonlinelibrary.com]
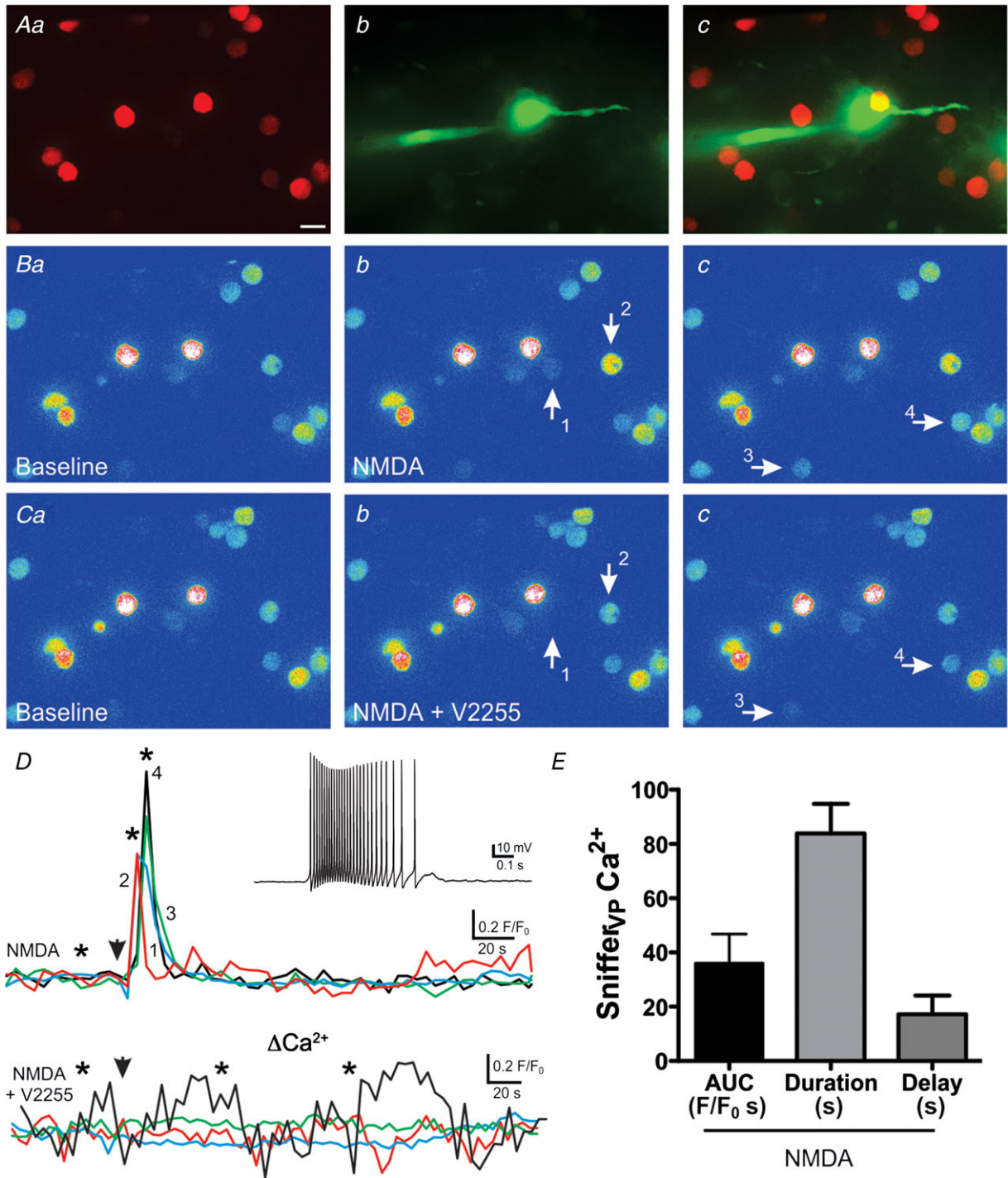
Figure 4. NMDA receptor activation evokes robust somatodendritic release of VP

A, fluorescence images of sniffer$_{VP}$ cells (*a*) surrounding a patched eGFP–VP neurone loaded with Alexa 488 (*b*). Both images are superimposed in *c*. *B*, corresponding pseudocolour images showing sniffer$_{VP}$ Ca^{2+} baseline (*a*) and responses in 4 cells (*b* and *c*, arrows) following focal application of NMDA (10 μM) to the patched neurone. *Ca–c*, NMDA stimulation to the same neurone failed to evoke sniffer$_{VP}$ cell responses in the presence of the V1aR antagonist V2255 (1 μM). *D*, plots of sniffer$_{VP}$ Ca^{2+} changes over time in the 4 cells shown in *B* and *C*, in the absence (upper panel) and presence (lower panel) of V2255. Arrowheads indicate the time of the NMDA stimulation, and asterisks correspond to the time points of the images shown in *Ba–c* and *Ca–c*. The inset shows the firing discharge of the patched neurone in response to NMDA stimulation. *E*, summary data of the mean area, duration and delay of sniffer$_{VP}$ responses to NMDAR-evoked firing in control ACSF (*n* = 21, from 10 patched eGFP–VP neurones). Scale bar: 15 μm. [Colour figure can be viewed at wileyonlinelibrary.com]

or the mean action potential frequency ($r^2 = 0.01$ and 0.002, respectively) evoked by NMDAR activation.

Similar experiments were repeated before and after bath application of a V1a receptor antagonist (V2255, 1 μM, $n = 5$ patched eGFP–VP neurones). As shown in the representative example of Fig. 4C and D, V2255 almost completely blocked sniffer$_{VP}$ Ca^{2+} responses to NMDAR activation (mean responsive sniffer$_{VP}$ cells: 3.20 ± 0.20 and 0.8 ± 0.58 for NMDA and NMDA+V2255, respectively; mean sniffer$_{VP}$ Ca^{2+} area: $49.4. \pm 18.4$ F/F_0 s and 2.9 ± 1.3 F/F_0 s for NMDA and NMDA+V2255, respectively $P < 0.01$ and 0.05, respectively). These results support that sniffer$_{VP}$ Ca^{2+} responses following NMDAR-evoked firing in VP neurones were mediated by endogenously released VP, and not by a direct effect of NMDA on the sniffer$_{VP}$ cells themselves.

To further confirm that the sniffer$_{VP}$ Ca^{2+} responses following focal application of NMDA resulted from stimulation of the patched eGFP–VP neurone rather than from stimulation of multiple VP neurones, we repeated a subset of experiments in which patched eGFP–VP neurones ($n = 9$) were dialysed with the Ca^{2+} chelator BAPTA (5 mM) and focally stimulated with NMDA as before. Sniffer$_{VP}$ cell responses in this condition were almost completely blocked, with only 2 out of 68 sampled sniffer cells showing a response (mean sniffer VP responses cells: 0.25 ± 0.15, $P < 0.001$ *vs.* NMDA (2.2 ± 0.45, see above). The number of responsive sniffer cells in BAPTA was too low to statistically compare the magnitude of the evoked response to that observed in NMDA).

Finally, it is worth noting that in a subset of experiments ($n = 9$) NMDAR-evoked depolarizations of eGFP–VP neurons were insufficient to evoke action potential firing. Nonetheless, Ca^{2+} responses in sniffer$_{VP}$ cell cells were still observed in 6/9 cases (Fig. 5). The magnitude (8.8 ± 2.2 F/F_0 s) and the duration (41.4 ± 4.7 s) of these responses, however, were significantly smaller than those cases in which NMDAR activation evoked action potentials (i.e. data shown Fig. 4E; $P < 0.05$ for both parameters, unpaired t test). No differences, however, in the delay were observed between the two conditions.

NMDAR-driven firing more efficiently evokes somatodendritic VP release than bursting or continuous intrinsic action potential firing within individual VP neurones

Our results support that NMDAR-evoked firing, compared to either RBF or CF modalities, more efficiently evokes somatodendritic neuropeptide release. In order to test this more directly, a combination of two or three of these different stimulation modalities, in which the sequence was randomly varied, were evoked in individually patched VP neurones in slices containing sniffer$_{VP}$ cells. We aimed to evoke a similar total number of action potentials with these various modalities. A representative example is shown in Fig. 6. In this case, focal application of NMDA evoked a burst of action potentials ($n = 120$ APs, 24 Hz), and with a delay of ~3 s, an increase in Ca^{2+} in three surrounding sniffer$_{VP}$ cell was observed (27.9 ± 8.9 F/F_0 s). When the same neurone was subjected to a CF modality ($n = 174$ APs, 27 Hz) no response was observed in any sniffer$_{VP}$ cells. Finally, when RBF activity was evoked ($n = 138$ APs, 21 Hz), a Ca^{2+} response was evoked only in one sniffer$_{VP}$ cell. This response, however, was markedly smaller (9.3 F/F_0 s) than those evoked by NMDAR activation, and occurred with a much more prolonged delay (~85 s).

In another representative example of a patched VP neurone (Fig. 7), we found that neither RBF ($n = 50$ APs, 8 Hz) nor CF modalities ($n = 41$ APs, 6 Hz) evoked Ca^{2+} responses in sniffer$_{VP}$ cells. Conversely, a smaller NMDAR-evoked burst of action potentials ($n = 16$, 1 Hz) evoked a robust Ca^{2+} response in seven sniffer$_{VP}$ cells (19.2 ± 2.3 F/F_0 s) with a delay of ~1 s after the stimulation. Similarly, another patched VP neurone subjected to a combination of NMDAR-evoked firing and a CF pattern (Fig. 8) showed that an NMDAR-mediated burst of action potentials ($n = 27$ APs, 7 Hz), evoked an increase in Ca^{2+} in five surrounding sniffer$_{VP}$ cells (13.8 ± 9.1 F/F_0 s, delay of ~3 s). Conversely, when CF activity was evoked with direct current injection ($n = 37$ APs, 12 Hz), a small response was observed in only one sniffer$_{VP}$ cell (4.1 F/F_0 s).

Figure 9 summarizes and compares sniffer$_{VP}$ cell responses among the three different firing modalities used to evoke firing in VP neurones. Overall, we found that the incidence of a successful release event (determined by a positive response in at least 1 sniffer$_{VP}$ cell) caused by NMDAR-evoked firing was significantly higher compared to both RBF and CF patterns ($P < 0.001$, chi-square test, Fig. 9A). Moreover, the mean number of responsive sniffer$_{VP}$ cells within each experiment was significantly higher in NMDAR-evoked firing, compared to CF and RBF patterns ($P < 0.01$ and $P < 0.05$, respectively, one-way ANOVA, Fig. 9B). Importantly, the magnitude of the sniffer$_{VP}$ cell response was also significantly larger in NMDAR-evoked firing, compared to RBF and CF patterns ($P < 0.01$ and $P < 0.001$, respectively, one-way ANOVA, Fig. 9C). Sniffer$_{VP}$ cell responses were also larger in the RBF compared to CF pattern, although the difference did not reach statistical significance ($P = 0.07$).

Even though we attempted to evoke a similar degree of firing in each condition, the RBF modality evoked a higher number of action potentials and firing frequencies compared to NMDA and CF modes ($P < 0.0001$, one-way ANOVA, Fig. 9D and E). However, the distribution histograms (see Fig. 9G and H) show overlapping ranges for the three modalities, and as

shown in the several individual examples shown (i.e. Figs 6–8), for similar number of evoked action potentials, NMDAR-evoked firing was more efficient than the other two firing modalities, and RBF more than CF, in evoking somatodendritic release of VP. This became also apparent when sniffer$_{VP}$ cell responses were normalized by the number of evoked spikes ($P < 0.001$, one-way ANOVA, not shown).

Another prominent difference among the various firing modalities was the delay from the initiation of the stimulus of the VP neurone until the sniffer$_{VP}$ Ca^{2+} response was observed. This delay was markedly shorter in NMDAR-evoked firing compared to RBF and CF patterns (Fig. 9F). Due to the low number of responses observed in the CF group ($n = 3$), we were only able to compute statistical differences between the NMDAR-evoked and the RBF mode ($P < 0.0001$).

When all data from the different stimulation protocols were combined, we found no significant correlations between the magnitude of the sniffer$_{VP}$ cell response with either the total number of action potentials ($r^2 = 0.04$, 0.04 and 0.07 for NMDA, RBF and CF, respectively) or the mean intraburst frequency ($r^2 = 0.002$, 0.009 and 0.05 for NMDA, RBF and CF, respectively) (Fig. 9G and H). Importantly, and as also highlighted in these plots, for

overlapping or even lower number of action potentials and firing frequencies, NMDAR-evoked firing resulted in a more robust sniffer$_{VP}$ cell response compared to RBF and CF patterns.

We also performed a running average of the mean sniffer$_{VP}$ Ca^{2+} response as a function of the number of evoked action potentials (bin = 10 APs) or the evoked firing frequencies (bin = 2.5 Hz). For NMDAR-evoked firing, we observed a bell-shaped curve for both action potential number and firing frequencies (Gaussian fit, $r^2 = 0.6$ and 0.7, respectively, Fig. 9I and J), suggesting an optimal dendritic release of VP in response to NMDAR activation at ~50 action potentials and ~15 Hz. Conversely, the RBF group only displayed a significant Gaussian distribution of sniffer$_{VP}$ Ca^{2+} response as a function of firing frequency ($r^2 = 0.8$, Fig. 9J), with an apparent optimal release at ~55 Hz. The low number of sniffer$_{VP}$ Ca^{2+} responses in the CF modality prevented us from performing a similar analysis for this group.

Taken together, these results support that for similar numbers of evoked action potentials or firing frequencies, NMDAR-evoked firing more efficiently stimulates somatodendritic release of VP. Our results also demonstrate that somatodendritic release is strengthened
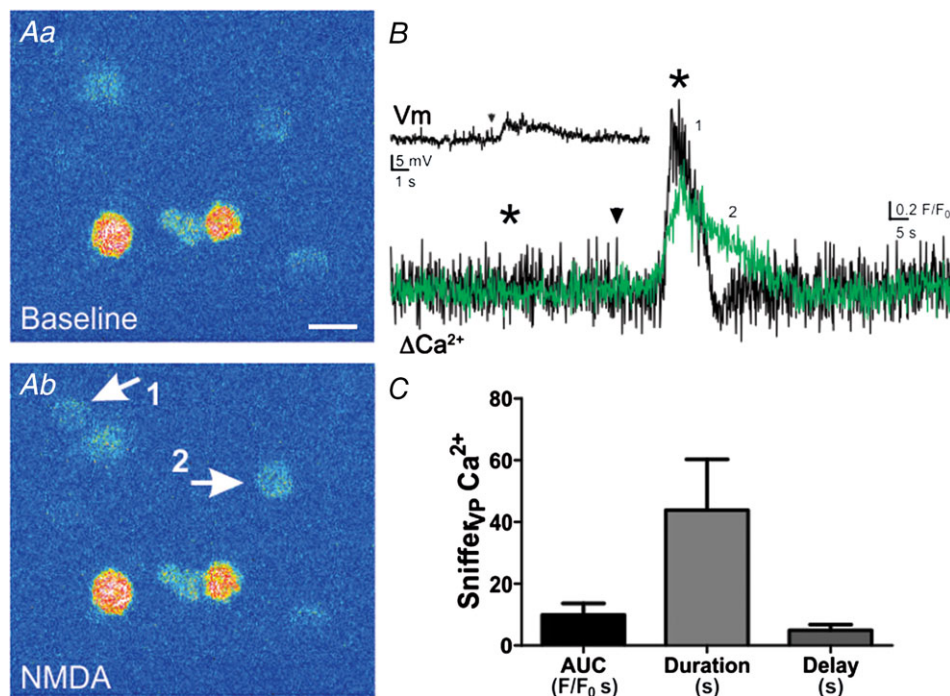
Figure 5. NMDAR activation evokes dendritic release of VP in the absence of action potentials
A, NMDA application (10 μM) caused a Ca^{2+} increase in 2 sniffer$_{VP}$ cells (arrows in *Ab*). This stimulus evoked a clear depolarization in the patched eGFP–VP neuron, which was insufficient, however, to evoke action potentials (*B* inset). *B*, traces show the changes in sniffer$_{VP}$ Ca^{2+} levels in both cells shown in *Ab*. Arrowheads show the time of NMDA application, and asterisks correspond to the time points of the images shown in *A*. *C*, summary data of mean area, duration and delay in response to NMDA without triggering action potentials ($n = 16$, from 6 patched eGFP–VP neurones). Scale bar: 15 μm. [Colour figure can be viewed at wileyonlinelibrary.com]

when action potentials are clustered in repetitive bursts, rather than in a continuous irregular pattern.

NMDAR-evoked action potentials are broader, but spike broadening is similar among stimulation modalities

In isolated axonal terminals, a progressive increase in action potential duration (i.e. spike broadening) has been shown to contribute to potentiated release evoked by clustered firing activity (Bicknell, 1988; Bourque, 1991). To determine whether NMDAR-evoked firing displayed more pronounced spike broadening compared to RBF or CF modes, we first compared the action potential waveform properties of individual spikes among groups, and then measured the mean action potential width for each of the first 10 action potentials of a train evoked in representative samples from each stimulation modality. As summarized in Table 1, the NMDAR-evoked action potential was significantly broader than that evoked during RBF and CF modalities ($P < 0.05$ *vs.* CF and RBF). Other action potential properties, including peak amplitude, rise and decay times, and the hyperpolarizing after-potential (HAP) were not different among groups. As shown in Fig. 10*A*, spike width progressively increased as a function of the action potential number within the train in all groups ($P < 0.0001$, two-way ANOVA). As with the single spike

analysis, we found that spike width remained significantly broader in NMDA-evoked spikes during the burst, compared to RBF or CF ($P < 0.001$, two-way ANOVA). To better quantify the degree and rate of spike broadening, spike widths within each train were normalized to the duration of the first spike in the train. As shown in Fig. 10*B*, we found no significant differences among groups in either spike broadening magnitude ($P = 0.5$, two-way ANOVA) or spike broadening rate (NMDAR: 0.05 ± 0.01 ms/spike; RBF: 0.05 ± 0.01 ms/spike; CF: 0.04 ± 0.01 ms/spike, $n = 6$/group, $P = 0.8$, one-way ANOVA).
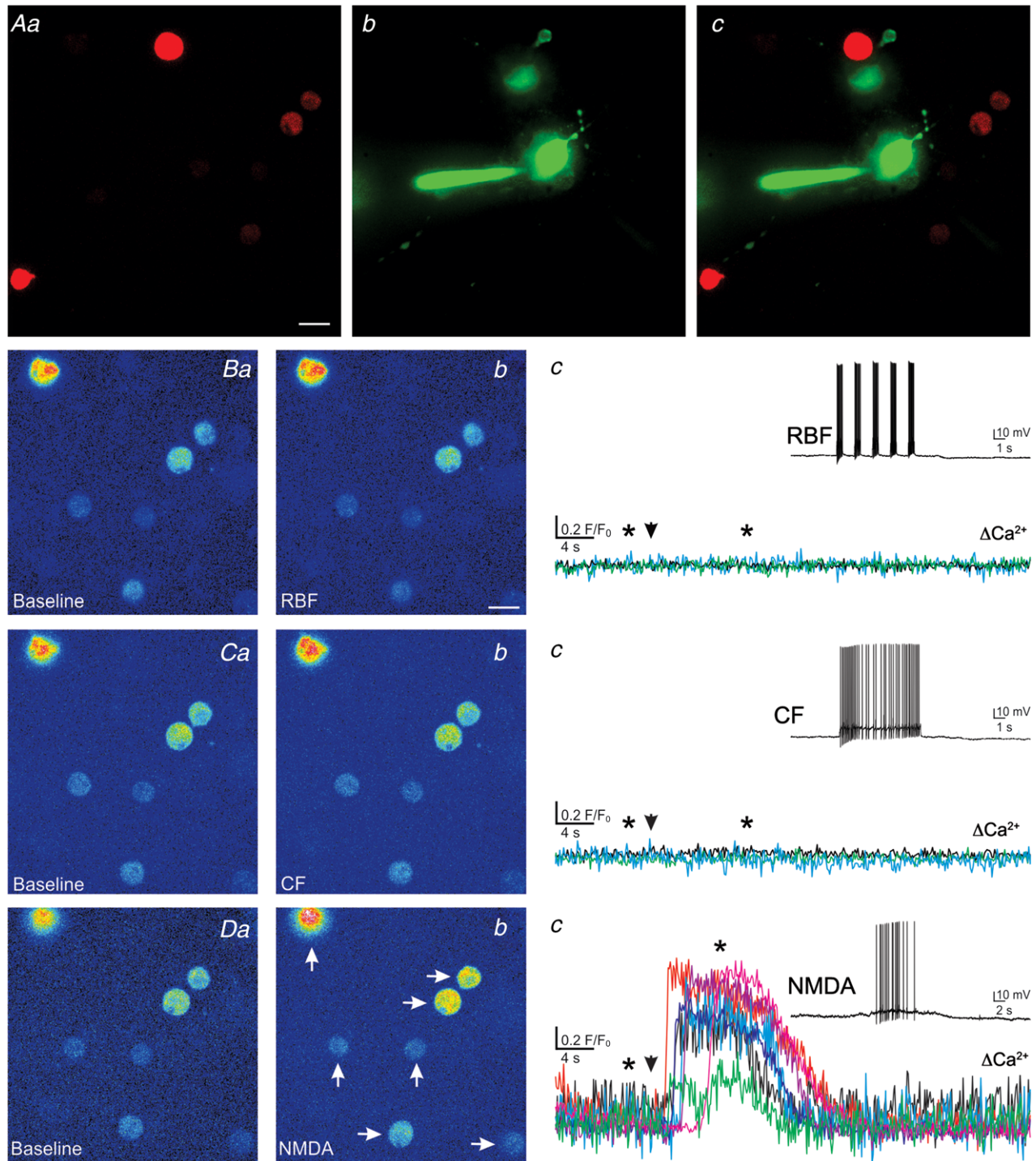
NMDAR boosting of somatodendritic release of VP is independent of the properties of evoked somatic firing activity

To determine if the more efficient somatodendritic release following NMDAR activation was dependent on a particular action potential waveform and/or firing pattern evoked, NMDA was focally applied to a subset of eGFP–VP neurones ($n = 5$), and the burst of evoked action potentials was then used as a voltage command waveform (VCW) to evoke the same firing response in the same neurone, but in the absence of NMDAR activation. The Ca^{2+} response in $sniffer_{VP}$ cells was assessed in response to both stimuli. As shown in Fig. 11, in this subset of experiments, NMDAR activation evoked bursts of action potentials (67.0 ± 15.9
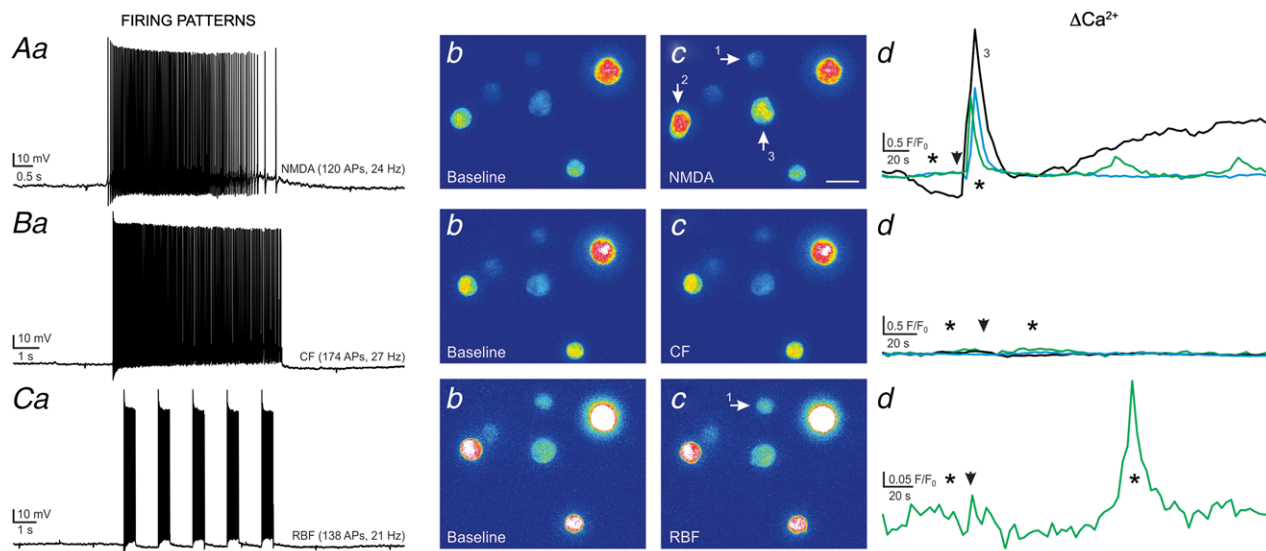
Figure 6. Somatodendritic release of VP is potentiated by NMDAR-evoked firing when compared to the other firing modalities elicited in the same VP neuron
A, NMDAR-evoked firing in a patched eGFP–VP neurone (NMDA 10 μM, *a*) resulted in positive Ca^{2+} responses in 3 $sniffer_{VP}$ cells (*b* and *c*, arrows). The corresponding Ca^{2+} plots are shown in *d*. *B*, a continuous firing discharge (CF) evoked in the same eGFP–VP neurone (40 pA, single depolarizing pulse, *a*) failed to generate $sniffer_{VP}$ responses (*b*–*d*). *C*, when the same eGFP–VP neurone was stimulated to evoke repetitive bursting firing (RBF, 80 pA, 5 depolarizing pulses, 0.5 s each, 1 s interval, *a*), a positive Ca^{2+} response was observed in only 1 $sniffer_{VP}$ cell (*b*–*d*). The magnitude and delay of this response was evidently smaller and longer compared to the response observed following NMDAR-evoked firing. Arrowheads in *Ad*, *Bd* and *Cd* show the time of the stimulation, and asterisks correspond to the time points of the images shown in panels *b* and *c*. [Colour figure can be viewed at wileyonlinelibrary.com]

Figure 7. Representative example showing a more robust somatodendritic release of VP evoked by NMDAR-mediated firing when compared to continuous or bursting firing in the same eGFP–VP neurone
A, fluorescence images of sniffer$_{VP}$ cells (*a*) in the vicinity of a patched eGFP–VP neurone loaded with Alexa 488 (*b*). Both images are superimposed in *c*. *B–D*, corresponding pseudocolour images showing basal (*a*) and sniffer$_{VP}$ Ca^{2+} responses when the patched neurone was stimulated to generate a RBF pattern (*Bb*), a CF pattern (*Cb*) or when firing was evoked by focal application of NMDA (10 μM, *Db*), in the sequence displayed. Plots of sniffer$_{VP}$ Ca^{2+} responses to each of the stimulation protocols are shown in panels *c*. Note that in this eGFP–VP neurone, only NMDAR-evoked firing resulted in robust Ca^{2+} responses in 7 different sniffer$_{VP}$ cells (arrows, *Db*). Arrowheads in panels *c* indicate the stimulation time, and asterisks correspond to the time points of the images shown in panels *a* and *b*. Scale bar: 15 μm. [Colour figure can be viewed at wileyonlinelibrary.com]

Table 1. Properties of action potentials evoked by the different stimulation modalities

| Stimulation modality	n	AP amplitude (mV)	AP half-width (ms)	AP rise (ms)	AP decay (ms)	HAP peak (mV)
NMDA	6	77.0 ± 4.3	1.20 ± 0.10	0.37 ± 0.04	1.26 ± 0.13	-26.3 ± 2.9
RBF	6	77.1 ± 3.8	0.83 ± 0.02**	0.39 ± 0.03	1.14 ± 0.16	-23.5 ± 2.9
CF	6	81.2 ± 33.6	0.93 ± 0.03*	0.35 ± 0.03	1.15 ± 0.14	-26.7 ± 2.8

Values are means $\pm$ SEM. *$P < 0.05$ and **$P < 0.01$ *vs* NMDA, one-way ANOVA. AP, action potential; CF, continuous firing; HAP, hyperpolarizing after-potential; RBF, repetitive bursting firing.

action potentials; 12.7 ± 3.5 Hz) that consistently evoked a Ca^{2+} response in sniffer$_{VP}$ cells (21.3 ± 6.7 F/F_0 s; mean delay: 5.2 ± 1.9 s; $n = 10$ sniffer$_{VP}$ cells). Surprisingly, however, when the same action potential firing activity was evoked using the VCW, no Ca^{2+} responses were observed in sniffer$_{VP}$ cells.

### NMDAR boosting of somatodendritic release of VP correlates with a larger dendritic Ca^{2+} signal in VP neurones

Somatodendritic release of neuropeptides involves Ca^{2+}-dependent exocytosis of LDCVs (Pow & Morris,

1989; Kennedy & Ehlers, 2011). Thus, we next assessed whether NMDAR-evoked firing resulted in larger changes in dendritic Ca^{2+} levels compared to RBF and CF modalities. To this end, we performed simultaneous patch-clamp and confocal Ca^{2+} imaging in eGFP–VP neurones loaded with the Ca^{2+}-sensitive dye Fluo5-F (50 μM), and neurones were stimulated with the three different firing modalities as used above (NMDA, RBF and CF). The mean number of evoked action potentials among the different firing modalities was not significantly different (NMDA: 71.1 ± 9.1 APs; RBF: 73.3 ± 7.6 APs; CF: 78.3 ± 8.9 APs, $P = 0.3$, one-way repeated measures ANOVA, $n = 8$). The dendritic Ca^{2+} measurements were
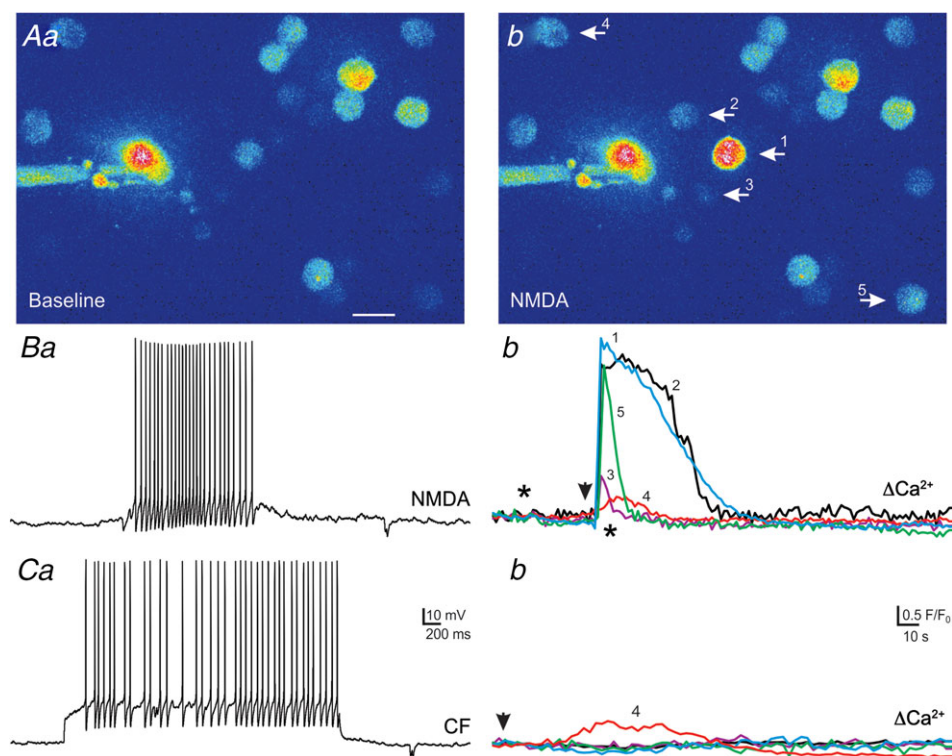
Figure 8. Another representative example showing a more robust somatodendritic release of VP evoked by NMDAR-mediated firing when compared to continuous firing mode in the same eGFP–VP neurone
A, pseudocolour images showing a patched eGFP–VP neurone surrounded by sniffer$_{VP}$ cells (*Aa* and *b*). Focally applied NMDA (10 μM) to the patched neurone evoked a burst of action potentials (27 APs, 7 Hz, *Ba*) that triggered a Ca^{2+} increase in 5 sniffer$_{VP}$ cells (arrows in *Ab*). *C*, a continuous firing pattern evoked by direct current injection (CF, 37 APs, 12 Hz, *Ca*) caused a Ca^{2+} response in only 1 sniffer$_{VP}$ cell (*Cb*). Arrowheads indicate the time of the stimulation and asterisks correspond to the time points of the images shown in *A*. Scale bar: 15 μm. [Colour figure can be viewed at wileyonlinelibrary.com]
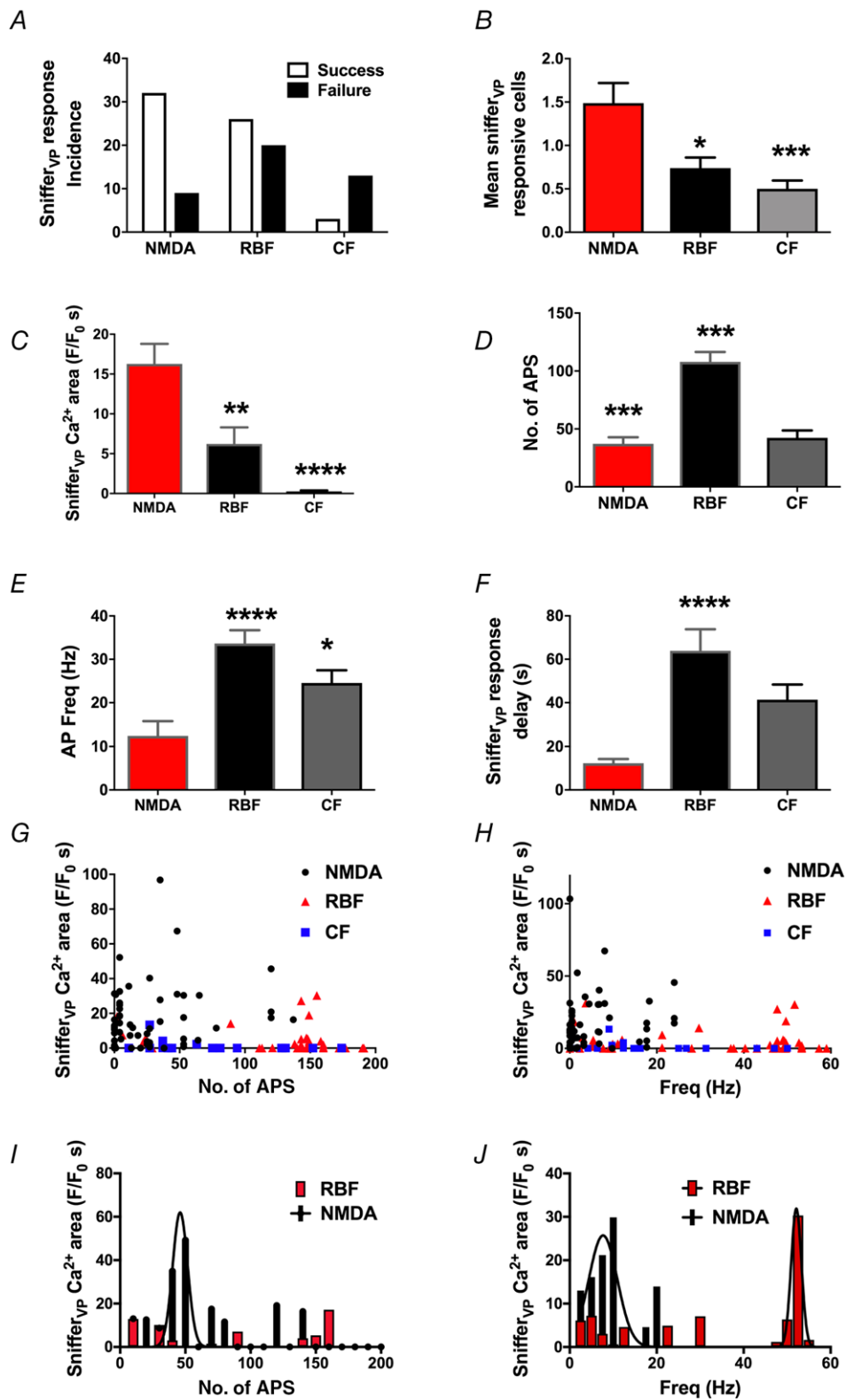
Figure 9. Summary of relationship between somatodendritic release of VP and the number and frequency of action potentials evoked with the three different firing modalities

A, the incidence of successful somatodendritic release events was significantly higher in NMDAR-evoked firing when compared to RBF or CF. *B* and *C*, summary of the mean number of sniffer_VP responsive cells (*B*) and sniffer_VP Ca^{2+} magnitude (area) (*C*) in response to the three stimulation modalities. *D* and *E*, summary of the

mean number of action potentials (*D*) and mean firing frequency (*E*) evoked by the three stimulation modalities in patched eGFP–VP neurons. *F*, summary of the mean sniffer$_{VP}$ Ca^{2+} response delay following stimulation of eGFP–VP neurones with the three different firing modalities. *G* and *H*, plots of sniffer$_{VP}$ Ca^{2+} responses (area) as a function of the number of APs (*G*) or action potential frequency (*H*). Note the lack of correlations observed in the three different stimulation modalities (no. of APs: $r^2 = 0.04$, 0.04 and 0.07 for NMDA, RBF and CF, respectively; frequency: $r^2 = 0.002$, 0.009 and 0.05 for NMDA, RBF and CF, respectively). *I*, plot showing a running average of the mean sniffer$_{VP}$ Ca^{2+} response as a function of the number of evoked APs (bin = 10 APs). The NMDAR-evoked, but not the RBF modality, was fit with a Gaussian function ($r^2 = 0.6$). *J*, plot showing a running average of the mean sniffer$_{VP}$ Ca^{2+} response as a function of the firing frequency (bin = 2.5 Hz). Both the NMDAR-evoked and the RBF modalities were fit with a Gaussian function ($r^2 = 0.7$ and 0.8, respectively). Note that the apparent optimal frequency for dendritic release in the case NMDAR-evoked firing was shifted towards lower firing frequencies compared to the RBF modality. *P < 0.05, **P < 0.01, ***P < 0.001 and ****P < 0.0001 vs NMDA (*B*, *C*, *E*, *F*) or vs. RBF (*D*), one-way ANOVA. For *A*, *D* and *E*: *n* (stimulated VP neurons) = 45, 46 and 30 for NMDA, RBF and CF, respectively. For *B*, *n* (individual sniffer$_{VP}$ cells) = 67, 54 and 15 for NMDA, RBF and CF, respectively. For *F*, *n* (individual sniffer$_{VP}$ cells with a positive response) = 47, 29 and 3 for NMDA, RBF and CF, respectively. [Colour figure can be viewed at wileyonlinelibrary.com]

obtained at a mean distance of 21.7 ± 2.3 μm from the soma, and were normalized by the corresponding total number of APs evoked in each stimulus. Changes in dendritic Ca^{2+} levels occurred almost instantaneously with the evoked firing activity, and no evident differences in the delay from stimulation to the evoked ΔCa^{2+} were observed. As shown in Fig. 12, we found that the increase in dendritic Ca^{2+} evoked by the CF and RBF patterns
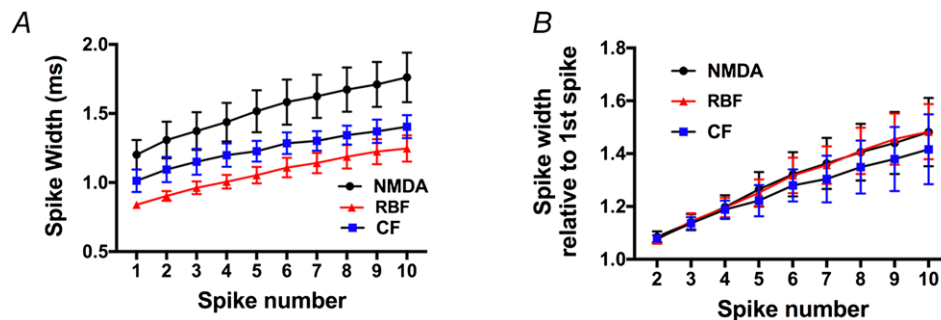
Figure 10. Spike broadening during repetitive firing was similar among the different stimulation modalities
A, plot of the mean spike width as a function of the action potential number within the train in all groups (*n* = 6/group). *B*, plot of the mean spike width normalized to the duration of the first spike of the train (*n* = 6/group). [Colour figure can be viewed at wileyonlinelibrary.com]
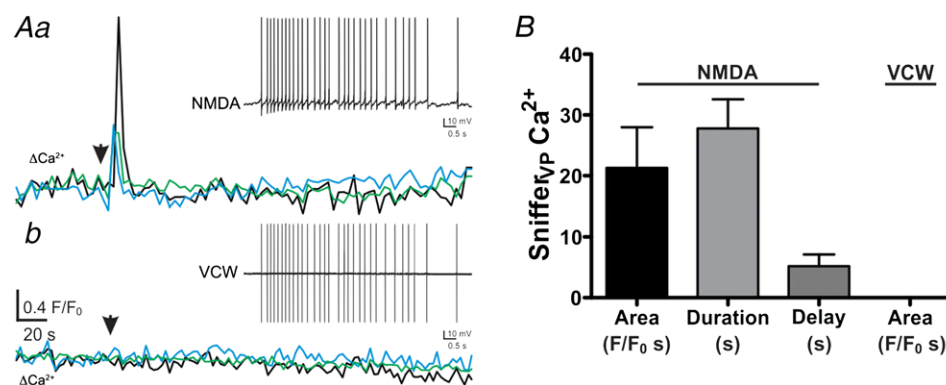
Figure 11. NMDAR facilitation of somatodendritic release of VP is not dependent of the properties of the evoked somatic firing activity
Aa, plots of Ca^{2+} changes over time recorded from 3 sniffer$_{VP}$ cells following focal application of NMDA (10 μM) to a recorded eGFP–VP neurone. The inset shows the firing response evoked in the patched neurone (31 APs, 3 Hz). *Ab*, the evoked activity in the patched neurone was then used as a voltage command waveform (VCW, inset) applied to the same neurone. The lower traces represent Ca^{2+} changes over time recorded from the same 3 sniffer$_{VP}$ cells as in *Aa* following the VCW stimulation. Note the lack of sniffer$_{VP}$ Ca^{2+} responses. *B*, summary data of the mean area, duration and delay in response to NMDA and VCW (*n* = 10 sniffer$_{VP}$ cells from 5 patched eGFP–VP neurons). [Colour figure can be viewed at wileyonlinelibrary.com]

were significantly smaller compared to the corresponding response evoked by NMDAR activation ($P < 0.002$, one-way repeated measures ANOVA).

We also compared changes in dendritic Ca^{2+} levels in neurones in which firing was evoked by NMDAR activation followed by the VCW, as described above. The increase in dendritic Ca^{2+} evoked by the VCW was also significantly smaller compared to the same firing evoked by NMDAR activation (NMDAR: 0.2 ± 0.04 F/F_0 s/APs;

VCW: 0.1 ± 0.02 F/F_0 s/APs $P < 0.05$ paired t test; $n = 10$).

Discussion

The precise mechanisms that couple firing activity and neuropeptide release, particularly from dendrites, remain poorly understood. Given that neuropeptides do not
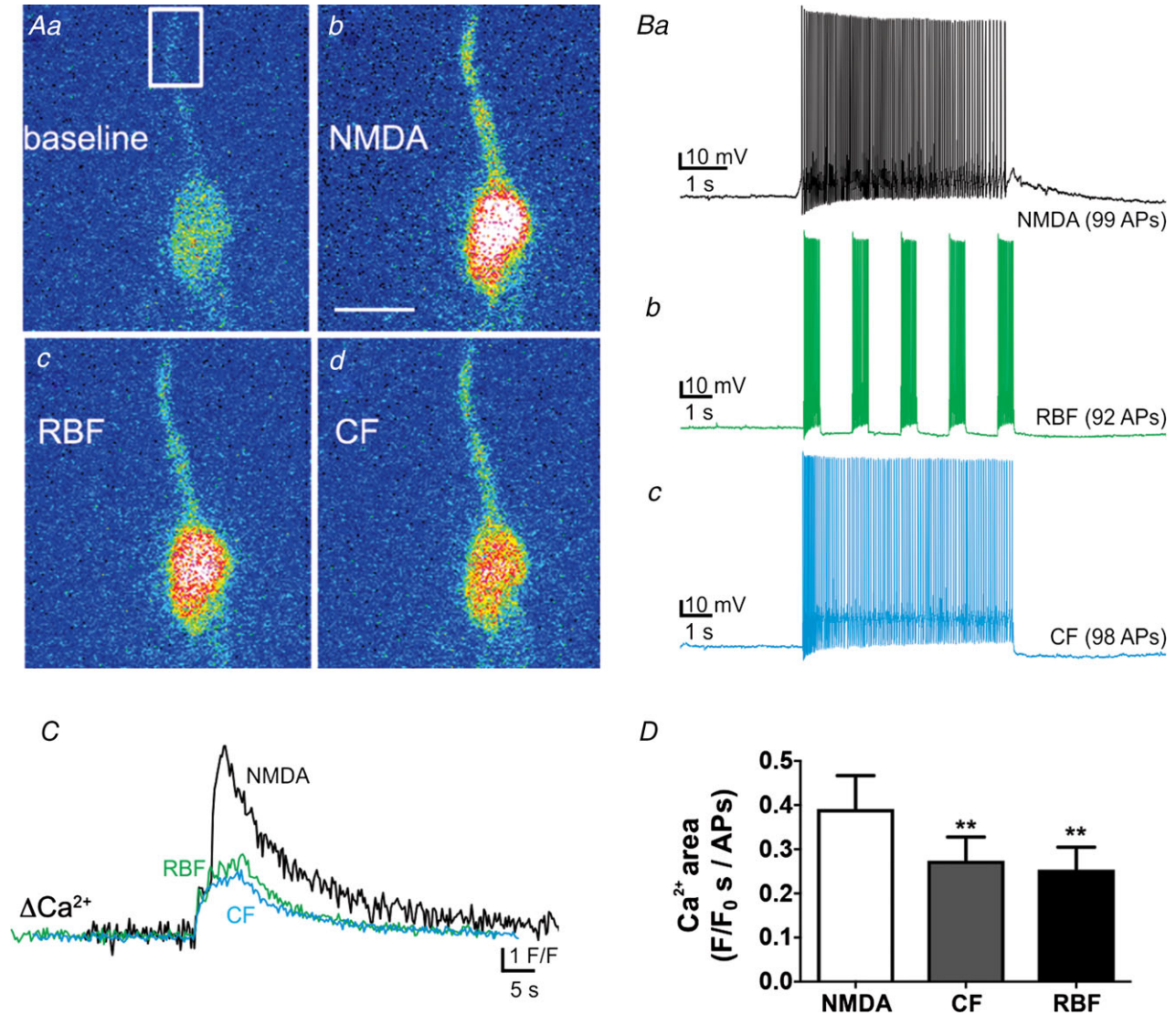
Figure 12. NMDAR-evoked firing results in larger increases in dendritic Ca^{2+} levels compared to continuous or repetitive bursting firing
A, representative pseudocolour confocal Ca^{2+} images of a patched eGFP–VP neurone dialysed with Fluo-5F showing somatodendritic Ca^{2+} changes in response to NMDAR-evoked firing (b), or direct current injection in repetitive bursting mode (RBF, c) and continuous mode (CF, d). B, electrophysiological recordings showing the firing activity evoked in this eGFP–VP neurone in response to NMDA (50 μM, Ba), RBF (b) and CF (c) modalities. In all cases we attempted to evoke approximately the same number of action potentials in each condition. C, plot of dendritic Ca^{2+} changes as a function of time in this eGFP–VP neurone in response to each firing modality. The Ca^{2+} signal was analysed in the region shown in Aa. Note the larger Ca^{2+} response to NMDAR activation compared to RBF and CF. D, summary data showing mean dendritic Ca^{2+} responses normalized by the number of action potentials evoked in each case ($n = 8$). **$P < 0.01$ vs. NMDA. Scale bar: 15 μm. [Colour figure can be viewed at wileyonlinelibrary.com]

evoke fast postsynaptic currents, their release cannot be readily detected with conventional electrophysiological approaches. Thus, microdialysis has been extensively used to measure brain neuropeptides (Ludwig *et al.* 1996; Landgraf & Neumann, 2004), albeit with poor temporal (tens of minutes) and spatial (1 mm^2) resolutions.

To overcome this limitation, we used 'sniffer' biosensor cells by genetically engineering CHO cells to express VP or OT receptors with a genetically encoded fluorescent Ca^{2+} indicator. Here, we show that sniffer$_{VP}$ responses were dose-dependent, with a threshold detection level of 0.5 nM and an EC_{50} of 7.2 nM for VP (which are similar to the previously reported binding affinity for V1a receptors; K_i of 4.2 nM; Mouillac *et al.* 1995), being thus an efficient tool to detect physiological levels of the neuropeptide. This was unequivocally shown by robust sniffer$_{VP}$ Ca^{2+} responses following activation of the VP neuronal population following an osmotic challenge, or by activation of a single VP neurone. A similar approach was recently used to detect axonal neuropeptide release (Pinol *et al.* 2014; Gizowski *et al.* 2016), and at the time of submission of this manuscript, a work was published that also demonstrated the efficient use of HEK cells transfected with GCaMP6 to detect both axonal and dendritic release of VP (Zaelzer *et al.* 2018). Thus, together with this present work, these studies strongly support sniffer cells as highly sensitive biosensors to quantitatively measure activity-dependent somatodendritic release of neuropeptides. Still, none of these previous studies addressed the role of different degrees and patterns of firing activity in regulating the efficacy of somatodendritic release of VP, which was a major goal of the present study.

An important limitation of the 'sniffer' cell approach that needs to be acknowledged is that it does not determine the precise location of the release event within the stimulated neurone. We attempted to improve this limitation by intracellularly loading the recorded VP neurone to better label the dendritic arbours. However, even in this condition, we rarely observed that responses in sniffer cells followed a specific spatial pattern in relation to the stimulated neurone. Whether this was due to technical limitations including incomplete dendritic staining and/or uneven distribution of sniffer cells around the patched neuron, or alternatively, whether this represents a random pattern by which released neuropeptides diffuse in the extracellular space, acting in a volume transmission manner (Ludwig & Leng, 2006; Son *et al.* 2013), is at present unknown. Irrespective of this, we did not attempt to make any conclusions regarding the specific site of release and/or diffusion patterns of released VP in the extracellular space. This limitation, however, did not compromise our ability to assess differences in the overall magnitude of somatodendritic release of VP, particularly when comparing responses to the different stimulation patterns within a single individual neurone.

Impact of different spiking properties and modalities on somatodendritic release of VP

Classical studies in isolated neurohypophysial terminals showed that axonal release of VP displays frequency-dependent facilitation (between 4 and 20 Hz), whereas spike clustering elicited more VP release than continuous firing (Dutton & Dyball, 1979; Cazalis *et al.* 1985; Bicknell, 1988; Bourque, 1991). Clustering and bursting firing may induce facilitation of axonal release via increased Ca^{2+} uptake at terminals (Cazalis *et al.* 1985), a phenomenon possibly associated to spike broadening, another frequency-dependent property of MNC axonal terminals (Bicknell, 1988; Bourque, 1991). Another beneficial aspect to clustering/bursting firing is that it minimizes secretory fatigue at axonal terminals (Cazalis *et al.* 1985; Bicknell, 1988). Thus, it is generally accepted that the typical clustered/phasic mode displayed by VP neurons in response to an osmotic challenge is best suited to optimize hormonal release at neurohypophysial axonal terminals.

While somatodendritic release of VP and OT is also activity-dependent (Ludwig *et al.* 2005), to what extend this process is influenced by the magnitude and/or pattern of somatic electrical activity, as summarized above for axonal terminals, is completely unknown. To address this fundamental question, we patched identified VP neurones in PVN slices containing sniffer$_{VP}$ cells. In quite a contrast to previous reports on axonal release (Dutton & Dyball, 1979; Cazalis *et al.* 1985; Bicknell, 1988), we found that continuous spiking activity over a broad range of spike numbers and frequencies failed to evoke any detactable somatodendritic release. Conversely, clustered firing activity evoked release in ∼60% of the cases, even from the same neurones that failed to release during continuous firing. No correlation between sniffer$_{VP}$ cell responses and either the total number or the frequency of evoked action potentials in clustered mode was observed. However, we found an optimal dendritic release of VP to occur with bursts of ∼55 Hz, which is considerably higher than that reported for axonal terminals (peaking at ∼15 Hz and displaying release fatigue at ∼50 Hz) (Dutton & Dyball, 1979; Bicknell, 1988). Our results clearly show that action potential clustering enhanced neuropeptide release from somatodendritic compartments. However, a limitation of our approach was that we used a single RBF protocol (i.e. 5 bursts), which was chosen based on our previous results showing that this pattern efficiently evoked an interpopulation crosstalk mediated by somatodendritic release of VP (Son *et al.* 2013). And while we were still able to evoke a wide range of total number of action potentials and firing frequencies with this protocol, it still remains to be determined more precisely whether the number of bursts *per se* influences the efficacy of somatodendritic release.

The present results also highlight the fact that neuropeptide stimulus–secretion coupling is less efficient in somatodendritic compartments compared to axons. To what extent these differences reflect limited ability of somatic action potentials to back-propagate into dendritic segments is at present unknown. MNCs express high levels of voltage-dependent, A-type K^+ channels (Luther *et al.* 2002), which were suggested to be more predominantly expressed in dendrites of MNCs (Widmer *et al.* 1997). Indeed, we found in a previous study that blockade of A-type K^+ channels in PVN neurons facilitated back-propagation of Ca^{2+} signals into dendritic compartments following somatic spikes (Sonner *et al.* 2010). Thus, future studies are also warranted to investigate the role of A-type K^+ channels in regulating stimulus–secretion coupling at dendritic compartments.

NMDAR-evoked firing boosts somatodendritic release of VP

NMDARs in MNCs promote clustered firing (Hu & Bourque, 1992; Bains & Ferguson, 1997; Gagnon *et al.* 2014) and evoke dendritic release of VP and OT (de Kock *et al.* 2004; Son *et al.* 2013). A major finding of our study was that NMDAR-mediated spiking significantly boosted dendritic release of VP, as shown by an increase in the percentage of positive release events observed (~80% cases), a significantly larger sniffer$_{VP}$ Ca^{2+} response, and a prominently shorter latency for the release event to occur, when compared to the other firing modalities. This potentiation was not due to more spikes and/or higher spike frequency elicited by NMDARs. In fact, a more robust NMDAR-evoked somatodendritic release was even observed at lower number of spikes or firing frequencies compared to the other modalities. We cannot completely rule out that the boosting effect of NMDA was due to activation of multiple VP neurones by the puff stimulation. This, however, was unlikely due to the fact that NMDA-evoked release was almost completely blocked when the patched neurone onto which the puff was focally directed was dialysed with the Ca^{2+} chelator BAPTA. Moreover, these results are in line with a recent study in which we found a similar boosting effect using a more precise, laser-evoked uncaging of NMDA, when compared to RBF firing (Son *et al.* 2013).

Activity-dependent somatodendritic release of VP occurred with a long latency after stimulation, which was significantly shortened when firing was evoked by NMDAR activation. Similar long latencies for neuropeptide release (up to 1 min) were reported in primary hippocampal cultures (Xia *et al.* 2009) and in endocrine cells (Chow *et al.* 1996; Elhamdani *et al.* 1998). The long latency reported here was unlikely due to a slow response of the sniffer cells, since they displayed a rapid response onset

when directly activated by the agonist. Moreover, since Ca^{2+} changes in dendrites exhibited almost no latency, and peaked within ~5 s following somatic firing, it is also unlikely that a slow dendritic invasion of electrical signals and/or Ca^{2+} was a contributing factor. Thus, similar to endocrine cells, long latencies for dendritic release could reflect lack of spatial localization between Ca^{2+} channels and dendritic LDCV.

NMDAR activation is necessary to evoke somatodendritic release of VP at physiological firing rates

Previous work elegantly demonstrated that axonal and dendritic release of neuropeptides from MNCs can occur in a compartmentalized manner and be regulated independently (Ludwig & Leng, 2006). Still, the mechanisms that contribute to this compartmentalized regulation remain unknown. VP neurones typically exhibit a phasic firing pattern, with firing rates of 8–15 Hz, a frequency known to optimize axonal release of VP (Dutton & Dyball, 1979; Brown & Bourque, 2006). We found that in response to NMDAR-evoked firing, an optimal dendritic release of VP occurred at ~15 Hz, which was markedly lower than that observed with the RBF modality, indicating that activation of NMDARs was necessary for dendritic release to occur at these physiological firing frequencies. Thus, depending on whether NMDARs are engaged or not, a particular firing discharge in VP neurones could result in somatodendritic and/or axonal release, respectively. Based on these results, we propose that NMDARs may act as a 'gating' mechanism, contributing to the differential regulation of neuropeptide release from these two neuronal compartments in MNCs.

Possible mechanisms underlying the potentiation of somatodendritic release of VP by NMDAR-evoked firing

We found that NMDAR-evoked action potentials were significantly broader compared to those evoked by direct current injection in either continuous or bursting modes. Broader spikes in MNCs reflect more Ca^{2+} influx *per* spike (Bourque & Renaud, 1985), a result that was also in line with the a larger increase in dendritic Ca^{2+} levels observed following NMDAR-evoked firing compared to RBF and CF modalities. Spike broadening, however, known to facilitate axonal release of neuropeptides from MNCs (Andrew & Dudek, 1985; Bourque & Renaud, 1985), was similar among the different firing modalities. Thus, to directly determine if differences in spike waveform and/or firing pattern evoked by NMDAR activation contributed to strengthening dendritic release of VP, we stimulated the same VP neurone with NMDA, and subsequently

used the evoked burst of action potentials as a VCW to evoke the same action potential/firing properties but in the absence of NMDAR activation. We reasoned that if the NMDAR-evoked single spike waveform and/or the firing pattern *per se* were sufficient to boost dendritic release of VP, the VCW should evoke a similar boosting effect. Surprisingly, however, we found that the VCW failed to evoke dendritic release of VP, suggesting that differences in spike width, spike broadening, or a particular firing pattern evoked by NMDAR activation were not critical factors contributing to their boosting effect. Similarly, since no differences in spike width (or action potential-evoked dendritic Ca^{2+} levels) were observed between RBF and CV modalities, these factors could not account for the enhanced somatodendritic release evoked by the former.

An important caveat to consider is that action potential invasion of dendrites could have been prevented during the VCW stimulation. However, the fact that rapid changes in dendritic Ca^{2+} levels, although of smaller magnitude, were still observed using the VCW argues against this possibility.

The smaller dendritic Ca^{2+} levels evoked with the VCW, however, suggest that sources other than action potentials themselves contributed to the overall enhanced dendritic Ca^{2+} signal following NMDAR activation. One likely additional source is Ca^{2+} influx through the NMDARs themselves, which was previously shown to contribute to the generation of dendritic Ca^{2+} spikes (Bains & Ferguson, 1999). In fact, our results showing that in some cases a sub-threshold depolarization evoked by NMDAR activation was sufficient to evoke dendritic release of VP, although to a significantly smaller degree than that observed in the presence of spikes, support an important contribution for NMDAR-mediated Ca^{2+} influx to the boosting effect on somatodendritic release mediated by NMDAR activation. Still, whether NMDAR-mediated dendritic Ca^{2+} influx results in a particular spatio-temporal profile of dendritic Ca^{2+} that leads to a faster and more efficient dendritic release of VP, possibly by mobilizing a readily releasable pool of LDCVs, will remain to be determine in future studies.

Finally, we recently showed that in addition to synaptically located NMDARs, MNCs also express functional extrasynaptic NMDARs that robustly influence MNCs' excitability and firing activity (Fleming *et al.* 2011), and that these receptors are coupled to distinct signalling cascades from their synaptic counterparts (Potapenko *et al.* 2012; Naskar & Stern, 2014). Extrasynaptic NMDARs are activated by ambient extracellular glutamate whose levels are independent of the degree of synaptic activity, but tightly controlled by astroglial glutamate transporters (Fleming *et al.* 2011; Potapenko *et al.* 2012). Importantly, the degree of neuronal coverage by glial processes in the magnocellular system (Perlmutter *et al.* 1985; Oliet *et al.* 2001), and thus the ability of glial glutamate trans-porters to restrict activation of extrasynaptic NMDARs by ambient glutamate (Fleming *et al.* 2011; Joe *et al.* 2014), changes in a state-dependent manner (i.e. during dehydration or lactation). Thus, it will be important in future studies to determine the relative contribution of synaptic and extrasynaptic NMDARs to dendritic release of VP under basal and physiologically challenging conditions.

In summary, our studies support sniffer cells as highly efficient biosensors to quantitatively monitor central release of neuropeptides. Moreover, we provide novel information regarding precise mechanisms that control somatodendritic release of neuropeptides known to be involved in critical physiological and behavioural functions.

References

Albers HE (2015). Species, sex and individual differences in the vasotocin/vasopressin system: relationship to neurochemical signaling in the social behavior neural network. *Front Neuroendocrinol* **36**, 49–71.

Andrew RD & Dudek FE (1985). Spike broadening in magnocellular neuroendocrine cells of rat hypothalamic slices. *Brain Res* **334**, 176–179.

Bains JS & Ferguson AV (1997). Nitric oxide regulates NMDA-driven GABAergic inputs to type I neurones of the rat paraventricular nucleus. *J Physiol* **499**, 733–746.

Bains JS & Ferguson AV (1999). Activation of N-methyl-D-aspartate receptors evokes calcium spikes in the dendrites of rat hypothalamic paraventricular nucleus neurons. *Neuroscience* **90**, 885–891.

Bicknell R (1988). Optimizing release from peptide hormone secretory nerve terminals. *J Exp Biol* **139**, 51–65.

Bourque CW (1991). Activity-dependent modulation of nerve terminal excitation in a mammalian peptidergic system. *Trends Neurosci* **14**, 28–30.

Bourque CW & Renaud LP (1985). Activity dependence of action potential duration in rat supraoptic neurosecretory neurones recorded in vitro. *J Physiol* **363**, 429–439.

Brown CH & Bourque CW (2006). Mechanisms of rhythmogenesis: insights from hypothalamic vasopressin neurons. *Trends Neurosci* **29**, 108–115.

Cazalis M, Dayanithi G & Nordmann JJ (1985). The role of patterned burst and interburst interval on the excitation-coupling mechanism in the isolated rat neural lobe. *J Physiol* **369**, 45–60.

Cheramy A, Leviel V & Glowinski J (1981). Dendritic release of dopamine in the substantia nigra. *Nature* **289**, 537–542.

Chow RH, Klingauf J, Heinemann C, Zucker RS & Neher E (1996). Mechanisms determining the time course of secretion in neuroendocrine cells. *Neuron* **16**, 369–376.

de Kock CP, Burnashev N, Lodder JC, Mansvelder HD & Brussaard AB (2004). NMDA receptors induce somatodendritic secretion in hypothalamic neurones of lactating female rats. *J Physiol* **561**, 53–64.

Dutton A & Dyball RE (1979). Phasic firing enhances vasopressin release from the rat neurohypophysis. *J Physiol* **290**, 433–440.

Elhamdani A, Zhou Z & Artalejo CR (1998). Timing of dense-core vesicle exocytosis depends on the facilitation L-type Ca channel in adrenal chromaffin cells. *J Neurosci* **18**, 6230–6240.

Engelmann M, Ludwig M & Landgraft R (1994). Simultaneous monitoring of intracerebral release and behavior: endogenous vasopressin improves social recognition. *J Neuroendocrinol* **6**, 391–395.

Fleming TM, Scott V, Naskar K, Joe N, Brown CH & Stern JE (2011). State-dependent changes in astrocyte regulation of extrasynaptic NMDA receptor signalling in neurosecretory neurons. *J Physiol* **589**, 3929–3941.

Filosa JA, Naskar K, Perfume G, Iddings JA, Biancardi VC, Vatta MS & Stern JE (2012). Endothelin-mediated calcium responses in supraoptic nucleus astrocytes influence magnocellular neurosecretory firing activity. *J Neuroendocrinol* **24**, 378–392.

Gagnon A, Walsh M, Okuda T, Choe KY, Zaelzer C & Bourque CW (2014). Modulation of spike clustering by NMDA receptors and neurotensin in rat supraoptic nucleus neurons. *J Physiol* **592**, 4177–4186.

Gizowski C, Zaelzer C & Bourque CW (2016). Clock-driven vasopressin neurotransmission mediates anticipatory thirst prior to sleep. *Nature* **537**, 685–688.

Gouzenes L, Desarmenien MG, Hussy N, Richard P & Moos FC (1998). Vasopressin regularizes the phasic firing pattern of rat hypothalamic magnocellular vasopressin neurons. *J Neurosci* **18**, 1879–1885.

Hu B & Bourque CW (1992). NMDA receptor-mediated rhythmic bursting activity in rat supraoptic nucleus neurones in vitro. *J Physiol* **458**, 667–687.

Joe N, Scott V & Brown CH (2014). Glial regulation of extrasynaptic NMDA receptor-mediated excitation of supraoptic nucleus neurones during dehydration. *J Neuroendocrinol* **26**, 35–42.

Kennedy MJ & Ehlers MD (2011). Mechanisms and function of dendritic exocytosis. *Neuron* **69**, 856–875.

Landgraf R & Neumann ID (2004). Vasopressin and oxytocin release within the brain: a dynamic concept of multiple and variable modes of neuropeptide communication. *Front Neuroendocrinol* **25**, 150–176.

Ludwig M, Bull PM, Tobin VA, Sabatier N, Landgraf R, Dayanithi G & Leng G (2005). Regulation of activity-dependent dendritic vasopressin release from rat supraoptic neurones. *J Physiol* **564**, 515–522.

Ludwig M, Callahan MF & Morris M (1995). Effects of tetrodotoxin on osmotically stimulated central and peripheral vasopressin and oxytocin release. *Neuroendocrinology* **62**, 619–627.

Ludwig M, Callahan MF, Neumann I, Landgraf R & Morris M (1994). Systemic osmotic stimulation increases vasopressin and oxytocin release within the supraoptic nucleus. *J Neuroendocrinol* **6**, 369.

Ludwig M & Leng G (1997). Autoinhibition of supraoptic nucleus vasopressin neurons in vivo: a combined retrodialysis/electrophysiological study in rats. *Eur J Neurosci* **9**, 2532–2540.

Ludwig M & Leng G (2006). Dendritic peptide release and peptide-dependent behaviours. *Nat Rev Neurosci* **7**, 126–136.

Ludwig M, Williams K, Callahan MF & Morris M (1996). Salt loading abolishes osmotically stimulated vasopressin release within the supraoptic nucleus. *Neurosci Lett* **215**, 1–4.

Luther JA, Daftary SS, Boudaba C, Gould GC, Halmos KC & Tasker JG (2002). Neurosecretory and non-neurosecretory parvocellular neurones of the hypothalamic paraventricular nucleus express distinct electrophysiological properties. *J Neuroendocrinol* **14**, 929–932.

Luther JA & Tasker JG (2000). Voltage-gated currents distinguish parvocellular from magnocellular neurones in the rat hypothalamic paraventricular nucleus. *J Physiol* **523 Pt 1**, 193–209.

Manning M, Misicka A, Olma A, Bankowski K, Stoev S, Chini B, Durroux T, Mouillac B, Corbani M & Guillon G (2012). Oxytocin and vasopressin agonists and antagonists as research tools and potential therapeutics. *J Neuroendocrinol* **24**, 609–628.

Morris JF & Ludwig M (2004). Magnocellular dendrites: prototypic receiver/transmitters. *J Neuroendocrinol* **16**, 403–408.

Mouillac B, Chini B, Balestre MN, Elands J, Trumpp-Kallmeyer S, Hoflack J, Hibert M, Jard S & Barberis C (1995). The binding site of neuropeptide vasopressin V1a receptor. Evidence for a major localization within transmembrane regions. *J Biol Chem* **270**, 25771–25777.

Naskar K & Stern JE (2014). A functional coupling between extrasynaptic NMDA receptors and A-type K$^+$ channels under astrocyte control regulates hypothalamic neurosecretory neuronal activity. *J Physiol* **592**, 2813–2827.

Oliet SH, Piet R & Poulain DA (2001). Control of glutamate clearance and synaptic efficacy by glial coverage of neurons. *Science* **292**, 923–926.

Perlmutter L, Tweedle C & Hatton G (1985). Neuronal/glial plasticity in the supraoptic dendritic zone in response to acute and chronic dehydration. *Brain Res* **361**, 225.

Pinol RA, Jameson H, Popratiloff A, Lee NH & Mendelowitz D (2014). Visualization of oxytocin release that mediates paired pulse facilitation in hypothalamic pathways to brainstem autonomic neurons. *PLoS One* **9**, e112138.

Potapenko ES, Biancardi VC, Zhou Y & Stern JE (2012). Astrocytes modulate a postsynaptic NMDA–GABA$_A$-receptor crosstalk in hypothalamic neurosecretory neurons. *J Neurosci* **33**, 631–640.

Pow DV & Morris JF (1989). Dendrites of hypothalamic magnocellular neurons release neurohypophysial peptides by exocytosis. *Neuroscience* **32**, 435–439.

Rice ME & Patel JC (2015). Somatodendritic dopamine release: recent mechanistic insights. *Philos Trans R Soc Lond B Biol Sci* **370**, 20140185.

Sabatier N, Shibuya I & Dayanithi G (2004). Intracellular calcium increase and somatodendritic vasopressin release by vasopressin receptor agonists in the rat supraoptic nucleus: involvement of multiple intracellular transduction signals. *J Neuroendocrinol* **16**, 221–236.

Son SJ, Filosa JA, Potapenko ES, Biancardi VC, Zheng H, Patel KP, Tobin VA, Ludwig M & Stern JE (2013). Dendritic peptide release mediates interpopulation crosstalk between neurosecretory and preautonomic networks. *Neuron* **78**, 1036–1049.

Sonner PM, Lee S, Ryu PD, Lee SY & Stern JE (2010). Imbalanced K^+ and Ca^{2+} subthreshold interactions contribute to increased hypothalamic presympathetic neuronal excitability in hypertensive rats. *J Physiol* **589**, 667–683.

Stern JE & Potapenko ES (2013). Enhanced NMDA receptor-mediated intracellular calcium signaling in magnocellular neurosecretory neurons in heart failure rats. *Am J Physiol Regul Integr Comp Physiol* **305**, R414–R422.

Stuart G, Spruston N, Sakmann B & Hausser M (1997). Action potential initiation and backpropagation in neurons of the mammalian CNS. *Trends Neurosci* **20**, 125–131.

Toida K, Kosaka K, Heizmann CW & Kosaka T (1994). Synaptic contacts between mitral/tufted cells and GABAergic neurons containing calcium-binding protein parvalbumin in the rat olfactory bulb, with special reference to reciprocal synapses between them. *Brain Res* **650**, 347–352.

Ueta Y, Fujihara H, Serino R, Dayanithi G, Ozawa H, Matsuda K, Kawata M, Yamada J, Ueno S, Fukuda A & Murphy D (2005). Transgenic expression of enhanced green fluorescent protein enables direct visualization for physiological studies of vasopressin neurons and isolated nerve terminals of the rat. *Endocrinology* **146**, 406–413.

Widmer H, Boissin-Agasse L, Richard P & Desarmenien MG (1997). Differential distribution of a potassium current in immunocytochemically identified supraoptic magnocellular neurones of the rat. *Neuroendocrinology* **65**, 229–237.

Xia X, Lessmann V & Martin TF (2009). Imaging of evoked dense-core-vesicle exocytosis in hippocampal neurons reveals long latencies and kiss-and-run fusion events. *J Cell Sci* **122**, 75–82.

Zaelzer C, Gizowski C, Salmon CK, Murai KK & Bourque CW (2018). Detection of activity-dependent vasopressin release from neuronal dendrites and axon terminals using sniffer cells. *J Neurophysiol* **203**, 1386–1396.

Additional information

Competing interests

All authors acknowledge that they there are no conflict of interests to disclose in accordance with the Journal policy.

Author contributions

S.P. M.Z. and E.C conducted experiments. S.P and J.E.S. designed the experiments and wrote the manuscript. All authors have read and approved the final version of this manuscript and agree to be accountable for all aspects of the work in ensuring that questions related to the accuracy or integrity of any part of the work are appropriately investigated and resolved. All persons designated as authors qualify for authorship, and all those who qualify for authorship are listed.

Funding

Acknowledgements